

Correlations of the elements of the neutrino mass matrix

W. Grimus^{*} and P.O. Ludl[†]

University of Vienna, Faculty of Physics
Boltzmanngasse 5, A-1090 Vienna, Austria

20 December 2012

Abstract

Assuming Majorana nature of neutrinos, we re-investigate, in the light of the recent measurement of the reactor mixing angle, the allowed ranges for the absolute values of the elements of the neutrino mass matrix in the basis where the charged-lepton mass matrix is diagonal. Apart from the derivation of upper and lower bounds on the values of the matrix elements, we also study their correlations. Moreover, we analyse the sensitivity of bounds and correlations to the global fit results of the neutrino oscillation parameters which are available in the literature.

^{*}E-mail: walter.grimus@univie.ac.at

[†]E-mail: patrick.ludl@univie.ac.at

1 Introduction

Our knowledge of the neutrino oscillation parameters has enormously improved in the recent years. The experimental results of the Double Chooz, Daya Bay and RENO Collaborations [1] have impressively confirmed the earlier hints [2] for a non-zero reactor mixing angle. Taking these novel results into account, the recent global fits [3, 4] establish $\theta_{13} > 0$ at a confidence level of $\sim 10\sigma$. Also the values of the solar mixing angle and the mass-squared differences are now known with good accuracy. While for a long time $\sin^2\theta_{23} \approx 1/2$ has been a very good approximation for the best fit value, the recent global fits [3, 4] hint towards a deviation from maximal atmospheric neutrino mixing. However, even at 1σ it is not clear from the recent fits in which octant θ_{23} lies. The global fit of [3] allows $\theta_{23} = 45^\circ$ at 2σ and that of [4] allows maximal atmospheric mixing within the 3σ range. The least known mixing parameter is the CP phase δ : it is unconstrained at 2σ , but the best fit values of [4] hint towards $\delta \approx \pi$.

With all these improved results, it is worthwhile to perform an investigation of the allowed ranges for the elements of the neutrino mass matrix \mathcal{M}_ν , as was done by Merle and Rodejohann in their seminal paper [5]. In the context of textures of \mathcal{M}_ν , the correlations of the elements $(\mathcal{M}_\nu)_{\alpha\beta}$ ($\alpha, \beta = e, \mu, \tau$) of the neutrino mass matrix are of particular interest. Therefore, the main goal of our paper is the construction of plots correlating the absolute values of the elements of the neutrino mass matrix with each other. We will assume Majorana nature of neutrinos in this paper.

The structure of our paper is as follows. In section 2 we investigate analytically upper and lower bounds on the absolute values of the elements of the neutrino mass matrix. In section 3 we will outline the numerical methods we will apply in our analysis, and the results will be presented in section 4. Finally we will draw conclusions in section 5.

2 The elements of the neutrino mass matrix

Assuming neutrinos to be of Majorana nature, the neutrino mass matrix is a complex symmetric 3×3 matrix, which can be diagonalized as

$$U^T \mathcal{M}_\nu U = \text{diag}(m_1, m_2, m_3), \quad (1)$$

where the m_i are the neutrino masses and U is a unitary matrix. In the following we will always assume to work in the basis in which the charged lepton mass matrix is given by

$$\mathcal{M}_\ell = \text{diag}(m_e, m_\mu, m_\tau), \quad (2)$$

which implies $U = U_{\text{PMNS}}$. Consequently, U can be decomposed as

$$U = D_1 V D_2, \quad (3)$$

where $D_1 = \text{diag}(e^{i\varphi_e}, e^{i\varphi_\mu}, e^{i\varphi_\tau})$ is a diagonal phase matrix, V is the mixing matrix in the parameterization suggested in [6], and $D_2 = \text{diag}(e^{i\sigma_1}, e^{i\sigma_2}, e^{i\sigma_3})$ is the matrix of Majorana phases. Without loss of generality, we assume $\sigma_3 = 0$. Inserting this into

equation (1) leads to

$$(\mathcal{M}_\nu)_{\alpha\beta} = (U^* \text{diag}(m_1, m_2, m_3) U^\dagger)_{\alpha\beta} = e^{-i(\varphi_\alpha + \varphi_\beta)} \sum_{k=1}^3 m_k e^{-2i\sigma_k} V_{\alpha k}^* V_{\beta k}. \quad (4)$$

The absolute values of the elements of the neutrino mass matrix

$$|(\mathcal{M}_\nu)_{\alpha\beta}| = |(\mathcal{M}_\nu^*)_{\alpha\beta}| = \left| \sum_k m_k e^{2i\sigma_k} V_{\alpha k} V_{\beta k} \right| \quad (5)$$

depend on nine real parameters, namely the three neutrino masses m_i , the three mixing angles θ_{12} , θ_{23} and θ_{13} , the Dirac CP phase δ and the two Majorana phases σ_1 and σ_2 .

From equation (5) we can deduce an upper bound on $|(\mathcal{M}_\nu)_{\alpha\beta}|$ as follows. Rewriting the absolute value as a scalar product

$$|(\mathcal{M}_\nu)_{\alpha\beta}| = \left| \sum_k m_k e^{2i\sigma_k} V_{\alpha k} V_{\beta k} \right| = \left| \sum_k \underbrace{\sqrt{m_k} e^{i\sigma_k} V_{\alpha k}}_{A_k^*} \underbrace{\sqrt{m_k} e^{i\sigma_k} V_{\beta k}}_{B_k} \right| \equiv |\langle A|B \rangle|, \quad (6)$$

we can use Cauchy-Schwarz's inequality to find

$$|(\mathcal{M}_\nu)_{\alpha\beta}| \leq |A| |B|. \quad (7)$$

Due to the unitarity of V , we have $\sum_k |V_{\alpha k}|^2 = 1$, and thus

$$|A| \leq \sqrt{\max_k m_k}, \quad |B| \leq \sqrt{\max_k m_k}, \quad (8)$$

which leads to the final result

$$|(\mathcal{M}_\nu)_{\alpha\beta}| \leq \max_k m_k, \quad (9)$$

i.e. the absolute value of an element of the neutrino mass matrix is smaller than the largest neutrino mass.

We can also construct a lower bound on $|(\mathcal{M}_\nu)_{\alpha\beta}|$. Defining

$$a_k \equiv m_k |V_{\alpha k}| |V_{\beta k}| \quad (10)$$

and taking into account that the Majorana phases are not constrained by experiment up to now, we find

$$|(\mathcal{M}_\nu)_{\alpha\beta}| = \left| \sum_{k=1}^3 e^{i\rho_k} a_k \right|, \quad (11)$$

where the ρ_k are unconstrained phases. Now we have to distinguish two cases. If the three numbers a_k are such that they can be conceived as the lengths of the sides of a triangle, then the right-hand side of equation (11) can become zero and $|(\mathcal{M}_\nu)_{\alpha\beta}|$ as well. It is easy to show that it is possible to construct a triangle with side lengths a_k , if and only if¹

$$2 \max_k a_k - \sum_k a_k \leq 0. \quad (12)$$

¹A different but equivalent inequality has been derived in [7].

Therefore, we end up with the inequality²

$$|(\mathcal{M}_\nu)_{\alpha\beta}| \geq 2 \max_k a_k - \sum_k a_k. \quad (13)$$

In this way, one gets rid of the Majorana phases and this inequality may be used to rule out single texture zeros in the neutrino mass matrix.

3 Numerical analysis

As already discussed in the previous section, the absolute values of the elements of \mathcal{M}_ν depend on nine variables, two of which—namely the two Majorana phases σ_1 and σ_2 —are totally unconstrained. In [5] the then available experimental data were used to produce plots of the $|(\mathcal{M}_\nu)_{\alpha\beta}|$ versus the smallest neutrino mass m_0 . The goal of the present paper is to produce—using the results of the latest global fits of neutrino oscillation experiments—plots of $|(\mathcal{M}_\nu)_{\alpha\beta}|$ versus $|(\mathcal{M}_\nu)_{\alpha'\beta'}|$. Since the knowledge of the neutrino oscillation parameters has improved considerably in the recent years, we also redo the numerical analysis of [5] and show the plots of $|(\mathcal{M}_\nu)_{\alpha\beta}|$ versus m_0 .

Let us now turn to our numerical strategy. Concerning the desired plots, a first attempt of creating scatterplots was, unfortunately, doomed to failure because even random point numbers as high as 10^9 were not sufficient to fathom enough of the allowed parameter space to achieve appealing plots. Therefore we follow a different strategy. From the scatterplots we can guess the shapes of the areas which would be filled in the limit of infinitely many points. In particular, we find that the allowed areas have no “holes,” from where it becomes clear that it is sufficient to construct their boundaries. We do this in the following way. Consider a plot showing $|(\mathcal{M}_\nu)_{\alpha\beta}|$ or m_0 on the x -axis and $|(\mathcal{M}_\nu)_{\alpha'\beta'}|$ on the y -axis. Then we start by pinning the quantity on the x -axis to some given value x_0 . Then we minimize and maximize y for fixed $x = x_0$ and obtain two points (x_0, y_{min}) and (x_0, y_{max}) of the boundary. Afterwards we do the same for fixed $y = y_0$ which leads to the two points (x_{min}, y_0) and (x_{max}, y_0) . Repeating this procedure with a suitable number of different values for x_0 and y_0 finally yields the desired allowed area.

As described above, we need an algorithm which allows to minimize and maximize real functions of nine variables.³ For this purpose we choose the Nelder–Mead algorithm (downhill simplex method) [8], which is a direct search method for finding a local minimum of a given function. However, since all functions f we will consider are non-negative, by minimizing $-f$ we can use the Nelder–Mead algorithm to find a local maximum of f . Since we are interested in the global minima (maxima) of f , single runs of the algorithm are not sufficient. Thus for every minimization (or maximization) we start with 200000 different random start simplices and also perform perturbations of candidates for a good minimum (maximum).

Since there are nine parameters in \mathcal{M}_ν , the domain of the Nelder–Mead algorithm is, by construction, the full parameter space \mathbb{R}^9 . In order to restrict the search to some

²If the right-hand side of inequality (13) is negative, then the resulting bound is $|(\mathcal{M}_\nu)_{\alpha\beta}| \geq 0$.

³Analysing the predictions of the “best fit” results of the global fits would reduce the number of parameters. However, instead of adapting our program to a smaller number of parameters, we let the parameters which shall assume their best fit values b vary in the interval $(b - \epsilon|b|, b + \epsilon|b|)$, with $\epsilon = 10^{-6}$.

domain $D \subset \mathbb{R}^9$, we decided for the following procedure. In the physical region, i.e. for an absolute neutrino mass scale of the order of at most $\sim \text{eV}$ (see the discussion at the end of this section), also the values of the function f to be minimized will be of the order of at most $\sim \text{eV}$. Therefore, instead of minimizing $f(p)$, we minimize $f(p) + \Pi_D(p)$, where $\Pi_D(p)$ is the characteristic function

$$\Pi_D(p) := \begin{cases} 0 \text{ eV} & \text{for } p \in D, \\ 10^6 \text{ eV} & \text{for } p \notin D. \end{cases} \quad (14)$$

Maximization of f is then equivalent to minimization of $\Pi_D - f$. The vector p collects the nine parameters of the $|(\mathcal{M}_\nu)_{\alpha\beta}|$. The pinning of x to x_0 is also achieved by adding a characteristic function, namely

$$\Pi_I(x(p)) := \begin{cases} 0 \text{ eV} & \text{for } x(p) \in I, \\ 10^6 \text{ eV} & \text{for } x(p) \notin I, \end{cases} \quad (15)$$

where I is an interval containing x_0 . The pinning of y to y_0 is done in the same way.

We also want to evaluate the lower bound (13) derived in section 2. For this purpose, we will use the Nelder–Mead algorithm on the function

$$2 \max_k a_k - \sum_k a_k + \Pi_D(p') \quad (16)$$

of the seven real variables $p' = (m_0, \Delta m_{21}^2, \Delta m_{31}^2, \theta_{12}, \theta_{23}, \theta_{13}, \delta)$.

Next let us discuss the domain D of the parameters p . For the mass-squared differences and the sines squared of the mixing angles we use the best fit as well as the $n\sigma$ -ranges ($n = 1, 2, 3$) provided by [3, 4]. The Majorana phases σ_1 and σ_2 are unconstrained and can thus vary between zero and 2π . The situation for δ is a bit ambiguous because the best fit values are very different in the two global fits [3] (version 3) and [4]; while for the normal ordering of the neutrino mass spectrum both fits favour a value of δ which is roughly π , the best fit values in the case of an inverted spectrum are ~ 0 and $\sim \pi$ for [3] (version 3) and [4], respectively. For this reason, in the “best fit”-plot we do not fix δ to its best fit value, but allow it to vary in its 1σ -range. Also for the 1σ -plots δ is allowed to vary in the respective 1σ -ranges; however, δ is unconstrained at the two and three sigma level.

The last parameter which remains to be discussed here, is the smallest neutrino mass m_0 . The strongest constraints on the absolute values of the neutrino masses comes from cosmology, where the sum of the light neutrino masses—in the form of the relic neutrino energy density Ω_ν —is one of the parameters of the standard model of cosmology [6]. There is no unique consensus on the resulting upper bound on $\sum_\nu m_\nu$, however most constraints are of the order of $\sum_\nu m_\nu < \mathcal{O}(1 \text{ eV})$ [6]. Therefore, we allow m_0 to vary between zero and 0.3 eV. In the limit of $m_0 \rightarrow 0.3 \text{ eV}$, this implies an upper bound on the largest neutrino mass of

$$\max_k m_k \lesssim m_0 + \frac{|\Delta m_{31}^2|}{2m_0} \approx 0.304 \text{ eV}. \quad (17)$$

According to equation (9), this directly translates to an upper bound of $\approx 0.3 \text{ eV}$ on the absolute values of the elements of the neutrino mass matrix.

		1σ	2σ	3σ
$ (\mathcal{M}_\nu)_{ee} $ (inv. spectrum)	Forero <i>et al.</i>	1.52×10^{-2}	1.36×10^{-2}	1.14×10^{-2}
	Fogli <i>et al.</i>	1.62×10^{-2}	1.44×10^{-2}	1.24×10^{-2}
$ (\mathcal{M}_\nu)_{\tau\tau} $ (norm. spectrum)	Forero <i>et al.</i>	0	0	0
	Fogli <i>et al.</i>	1.86×10^{-2}	1.27×10^{-2}	0

Table 1: Numerical results for the lower bounds on $|(\mathcal{M}_\nu)_{ee}|$ (inverted spectrum) and $|(\mathcal{M}_\nu)_{\tau\tau}|$ (normal spectrum) in units of eV using the global fits of Forero *et al.* (version 3) [3] and Fogli *et al.* [4]. The lower bounds for all other $|(\mathcal{M}_\nu)_{\alpha\beta}|$ are zero.

Assuming that the “standard mechanism” (induced by the Majorana mass term) dominates neutrinoless double beta decay, its non-observation gives upper bounds on $|(\mathcal{M}_\nu)_{ee}|$, the current bounds being of the order of [9, 10]

$$|(\mathcal{M}_\nu)_{ee}| \lesssim 0.4 \text{ eV}, \quad (18)$$

which is comparable to the cosmological bound. Thus, unfortunately, the bound (18) will be fulfilled automatically in our numerical analysis and will, therefore, give no additional constraint on $|(\mathcal{M}_\nu)_{ee}|$. However, the bound (18) implies an upper bound on the absolute neutrino mass scale [9]. Using the 3σ -ranges for the oscillation parameters one can estimate the bound to be [9]

$$m_0 \lesssim 1.9 \text{ eV}. \quad (19)$$

Here the constraints from cosmology are much stronger.

The bound on m_0 coming from tritium decay is of almost the same size as the one from neutrinoless double beta decay, namely $m_0 < 2 \text{ eV}$ [6], and will therefore not constrain the results of our analysis.

4 Results

Lower bounds on $|(\mathcal{M}_\nu)_{\alpha\beta}|$: Using inequality (13) and the global fits of [3, 4] shows that the only elements of $|(\mathcal{M}_\nu)_{\alpha\beta}|$ which have a non-trivial lower bound are $|(\mathcal{M}_\nu)_{ee}|$ in the case of an inverted neutrino mass spectrum and $|(\mathcal{M}_\nu)_{\tau\tau}|$ in the case of normal ordering of the neutrino masses. The resulting bounds can be found in table 1.

Let us compare these bounds with the results of the analysis of Merle and Rodejohann [5]. From the plots presented there one can read off that the only non-trivial lower bound on an element of \mathcal{M}_ν is the bound

$$|(\mathcal{M}_\nu)_{ee}| \geq 7 \times 10^{-3} \text{ eV} \quad (20)$$

in the case of an inverted neutrino mass spectrum. Note that with the present data this bound has improved by a factor of two (see table 1), corresponding to a factor four in the lifetime of neutrinoless double beta decay.

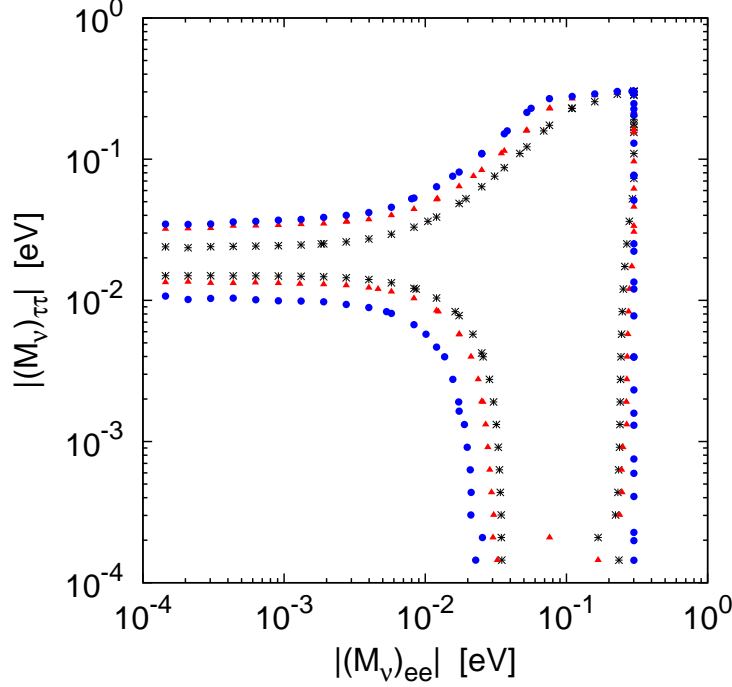


Figure 1: Allowed ranges for $|(\mathcal{M}_\nu)_{ee}|$ vs. $|(\mathcal{M}_\nu)_{\tau\tau}|$ in the case of a normal mass spectrum, using the global fit of Forero *et al.* (version 3). The best fit area is bounded by black stars, the 1σ area by red triangles, and the 3σ area by blue points.

How to read the plots: Before we discuss the resulting plots, we have to explain how they are to be read. This may best be done by means of an example. The properties we will outline in the following, hold for all plots in this paper.

Figure 1 shows the allowed areas for $|(\mathcal{M}_\nu)_{ee}|$ vs. $|(\mathcal{M}_\nu)_{\tau\tau}|$ in the case of a normal mass spectrum. The plot consists of three types of points, each one describing the boundary of an allowed area. The best fit area is bounded by black stars $*$, the 1σ area is bounded by red triangles \blacktriangle , and finally the 3σ area is bounded by blue points \bullet . Note that also the plot axes comprise parts of the boundaries of the allowed areas, as can be seen in figure 1. This feature is very pronounced for instance in figure 2.

In appendix A we present the plots based on the global fit of Fogli *et al.* The plots based on the global fits of Forero *et al.* (versions 2 and 3) are shown in appendices C and D, respectively.

Plots of the smallest neutrino mass versus $|(\mathcal{M}_\nu)_{\alpha\beta}|$: Concerning the plots of $|(\mathcal{M}_\nu)_{\alpha\beta}|$ as a function of the smallest neutrino mass, an interesting point is whether they have changed since the original analysis of Merle and Rodejohann [5] in 2006. The main difference is that at the time when reference [5] was written, only an upper bound on the size of θ_{13} was known, which is the reason that [5] contains plots for different sizes of $\sin^2 2\theta_{13}$. Comparing our plots to the ones of [5] with $\sin^2 2\theta_{13} = 0.1$, we find that at the 3σ level the plots in [5] are still in good agreement also with the new results. However, for the best fit only the plots of the smallest neutrino mass versus $|(\mathcal{M}_\nu)_{ee}|$ and $|(\mathcal{M}_\nu)_{\mu\tau}|$

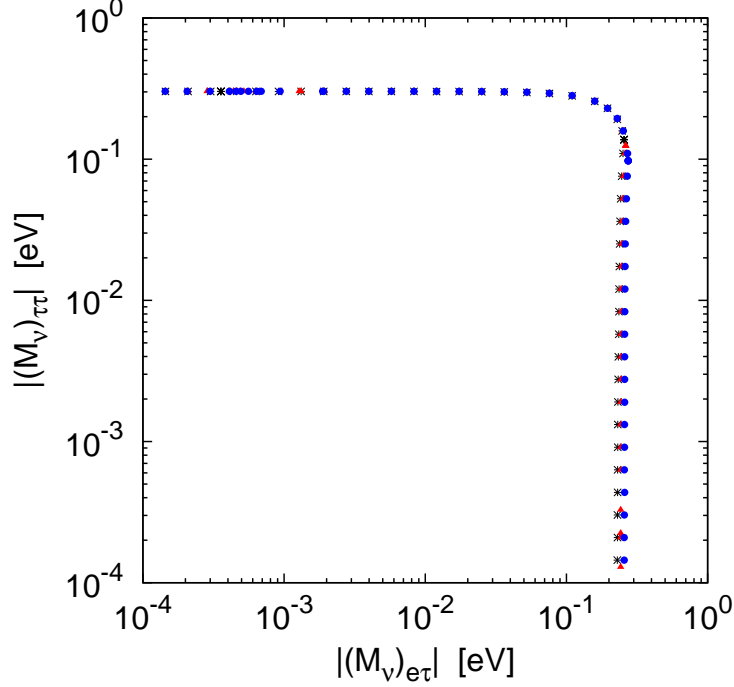


Figure 2: Allowed ranges for $|(\mathcal{M}_\nu)_{e\tau}|$ vs. $|(\mathcal{M}_\nu)_{\tau\tau}|$ in the case of a normal mass spectrum, using the global fit of Forero *et al.* (version 3). For more information *cf.* figure 1 and section 4.

are in good agreement with the plots obtained from the new data. The 1σ regions are not indicated in [5].

Finally, from the plots we can readily read off the lower bounds on the $|(\mathcal{M}_\nu)_{\alpha\beta}|$ and compare them with the bounds found from evaluating inequality (13)—see table 1. We find full agreement, which provides a successful consistency check of our results.

Plots of $|(\mathcal{M}_\nu)_{\alpha\beta}|$ versus $|(\mathcal{M}_\nu)_{\alpha'\beta'}|$: In this section we will discuss some of the conclusions one can draw from the correlation plots. These plots can be used to test the viability of two texture zeros in \mathcal{M}_ν . The results obtained from the plots are in perfect agreement with the results of a recent numerical analysis provided in [11], and may—at 3σ —be condensed to the fact that the seven two texture zeros originally presented in [12] are still viable with all of the three global fits [3, 4]. For further details we refer the reader to [11].

Let us continue by discussing those correlations which appear manifest at the 3σ level. Going through all the plots, we find the correlations

$ (\mathcal{M}_\nu)_{ee} $	vs.	$ (\mathcal{M}_\nu)_{\mu\mu} $	(normal spectrum)
$ (\mathcal{M}_\nu)_{ee} $	vs.	$ (\mathcal{M}_\nu)_{\mu\tau} $	(normal spectrum)
$ (\mathcal{M}_\nu)_{ee} $	vs.	$ (\mathcal{M}_\nu)_{\tau\tau} $	(normal spectrum)
$ (\mathcal{M}_\nu)_{\mu\mu} $	vs.	$ (\mathcal{M}_\nu)_{\mu\tau} $	(normal spectrum)
$ (\mathcal{M}_\nu)_{\mu\tau} $	vs.	$ (\mathcal{M}_\nu)_{\tau\tau} $	(normal spectrum)

most stringent. All these five correlations may be subsumed as follows: “If one matrix element is small, the other one must be large,” as can, for example, be seen from figure 1. However, there are also matrix elements which appear to be totally uncorrelated. A good example for this case is $|(\mathcal{M}_\nu)_{e\tau}|$ vs. $|(\mathcal{M}_\nu)_{\tau\tau}|$ in the case of a normal spectrum—see figure 2.

While at the 3σ level all plots produced using the three different global fits of Forero *et al.* and Fogli *et al.* agree very well, at the 1σ level this situation changes completely. Instead of presenting a confusing list showing all differences, let us just mention the most important point which is the fact that the fit results of Fogli *et al.* no longer allow a vanishing matrix element $|(\mathcal{M}_\nu)_{\tau\tau}|$ at 1σ in the case of a normal neutrino mass spectrum, while the fit results of Forero *et al.* still do. This evidently also has strong consequences on all correlation plots including $|(\mathcal{M}_\nu)_{\tau\tau}|$, a fine example being the plot of $|(\mathcal{M}_\nu)_{\mu\tau}|$ vs. $|(\mathcal{M}_\nu)_{\tau\tau}|$, which is shown in figure 3. See also the corresponding plot in appendix B.

Let us finally discuss the sensitivity of the correlation plots to the data. As already pointed out, correlations which contain $|(\mathcal{M}_\nu)_{\tau\tau}|$ are particularly sensitive, due to the strong constraint on $|(\mathcal{M}_\nu)_{\tau\tau}|$ in the case of a normal neutrino mass spectrum—see table 1. However, also for an inverted mass spectrum the plots involving $|(\mathcal{M}_\nu)_{\tau\tau}|$ differ visibly for the fits by Forero *et al.* (version 3) and Fogli *et al.* Other correlation plots which are quite sensitive to the data at 1σ are:

$ (\mathcal{M}_\nu)_{ee} $	vs.	$ (\mathcal{M}_\nu)_{e\tau} $	(normal spectrum)
$ (\mathcal{M}_\nu)_{ee} $	vs.	$ (\mathcal{M}_\nu)_{\mu\mu} $	(inverted spectrum)
$ (\mathcal{M}_\nu)_{e\mu} $	vs.	$ (\mathcal{M}_\nu)_{\mu\mu} $	(normal and inv. spectrum)
$ (\mathcal{M}_\nu)_{e\tau} $	vs.	$ (\mathcal{M}_\nu)_{\mu\mu} $	(normal and inv. spectrum)
$ (\mathcal{M}_\nu)_{\mu\mu} $	vs.	$ (\mathcal{M}_\nu)_{\mu\tau} $	(inverted spectrum)

Thus in total 17 out of the 30 possible correlations are particularly sensitive to the data at the 1σ level. In appendix B we provide the 17 corresponding plots showing the allowed 1σ regions for both Forero *et al.* (version 3) and Fogli *et al.*

5 Conclusions

In this paper, assuming Majorana neutrinos, we re-investigated the allowed ranges for the elements of the neutrino mass matrix in the light of the results of the recent global fits. In particular our analysis could profit from the fact that also the reactor mixing angle is by now well determined. In contrast, at the time of the original analysis by Merle and Rodejohann [5] only an upper bound on $\sin^2\theta_{13}$ was known.

By means of Cauchy-Schwarz’s inequality we could show that, in the basis where the charged lepton mass matrix is diagonal, the absolute value of an element of \mathcal{M}_ν cannot exceed the largest neutrino mass. The most stringent bound on the absolute neutrino mass scale coming from cosmology thus implies the bound

$$|(\mathcal{M}_\nu)_{\alpha\beta}| \lesssim 0.3 \text{ eV}. \quad (21)$$

We could also derive lower bounds on the elements of the neutrino mass matrix. Numerically evaluating these bounds on the basis of the global fits of oscillation data revealed

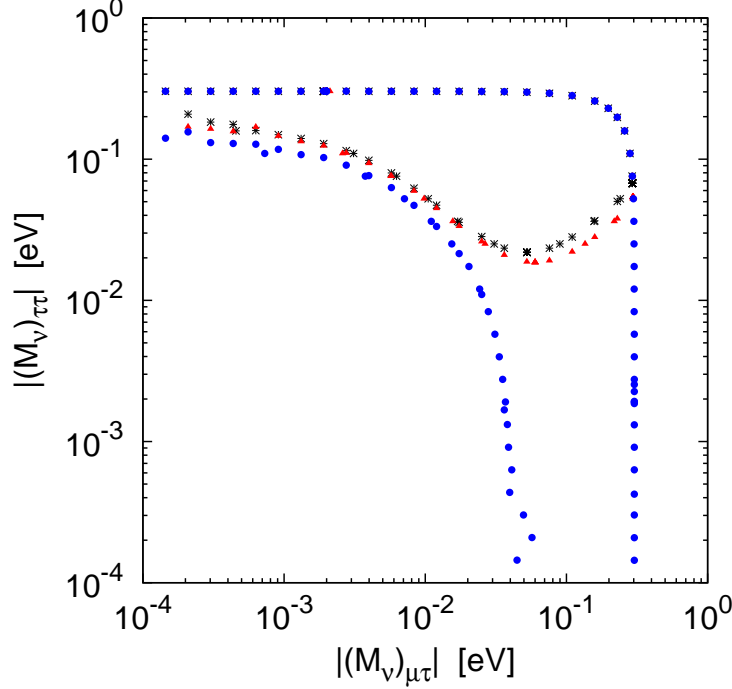


Figure 3: Allowed ranges for $|(\mathcal{M}_\nu)_{\mu\tau}|$ vs. $|(\mathcal{M}_\nu)_{\tau\tau}|$ in the case of a normal mass spectrum, using the fit results of Fogli *et al.* For more information *cf.* figure 1 and section 4.

that only for $|(\mathcal{M}_\nu)_{ee}|$ (inverted spectrum) and $|(\mathcal{M}_\nu)_{\tau\tau}|$ (normal spectrum) non-trivial lower bounds exist—see table 1. While the fact that $|(\mathcal{M}_\nu)_{ee}|$ is non-zero at 3σ was already clear in [5], the lower bound on $|(\mathcal{M}_\nu)_{\tau\tau}|$ is a feature of the new fit of Fogli *et al.* [4]. However the non-trivial bound is only valid at 2σ and the fits of Forero *et al.* [3] still allow zero $|(\mathcal{M}_\nu)_{\tau\tau}|$ even at 1σ .

The second main point of our analysis was the creation of correlation plots of the absolute values of the elements of \mathcal{M}_ν . We created plots based on three different global fits [3, 4] and found that at the 3σ level there is no discrepancy between the different global fits. For every global fit we obtained 30 correlation plots (15 correlations, two spectra). Among the 30 possibilities we found only five stringent correlations at the 3σ level, namely:

$ (\mathcal{M}_\nu)_{ee} $	vs.	$ (\mathcal{M}_\nu)_{\mu\mu} $	(normal spectrum)
$ (\mathcal{M}_\nu)_{ee} $	vs.	$ (\mathcal{M}_\nu)_{\mu\tau} $	(normal spectrum)
$ (\mathcal{M}_\nu)_{ee} $	vs.	$ (\mathcal{M}_\nu)_{\tau\tau} $	(normal spectrum)
$ (\mathcal{M}_\nu)_{\mu\mu} $	vs.	$ (\mathcal{M}_\nu)_{\mu\tau} $	(normal spectrum)
$ (\mathcal{M}_\nu)_{\mu\tau} $	vs.	$ (\mathcal{M}_\nu)_{\tau\tau} $	(normal spectrum)

All these correlations may be subsumed as: “If one matrix element is small, the other one must be large.”

While at the 3σ level the different global fits all agree, this is not so when one considers the 1σ level. There the most striking fact is that the fit of Fogli *et al.* [4] does no longer allow a vanishing matrix element $(\mathcal{M}_\nu)_{\tau\tau}$ at 1σ in the case of a normal mass spectrum.

In summary, we conclude that correlations evident at the 3σ level exist only for the normal mass spectrum. However, there are interesting features also at the 1σ level which may be corroborated (or refuted) by future experimental results increasing the accuracy of global fit data.

Acknowledgements: This work is supported by the Austrian Science Fund (FWF), Project No. P 24161-N16. P.O.L. thanks Andreas Singraber for fruitful discussions and helpful comments on the numerical part of this work and Helmut Moser for his tireless servicing of the institute's computer cluster on which the computations for this work were performed.

References

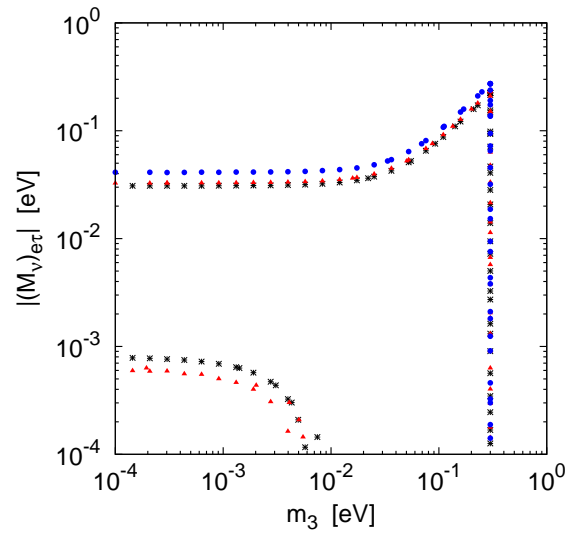
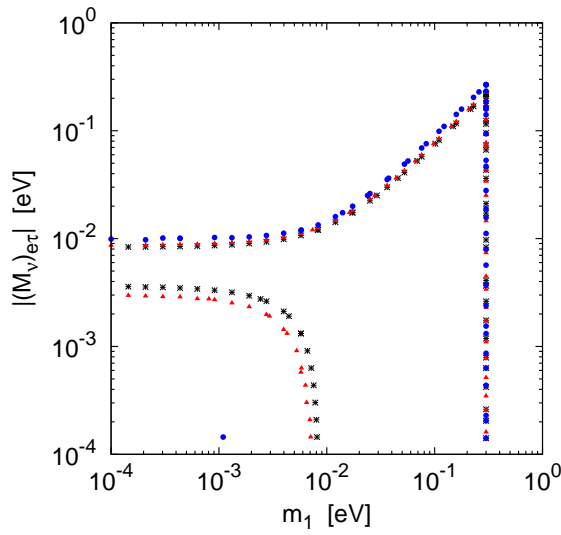
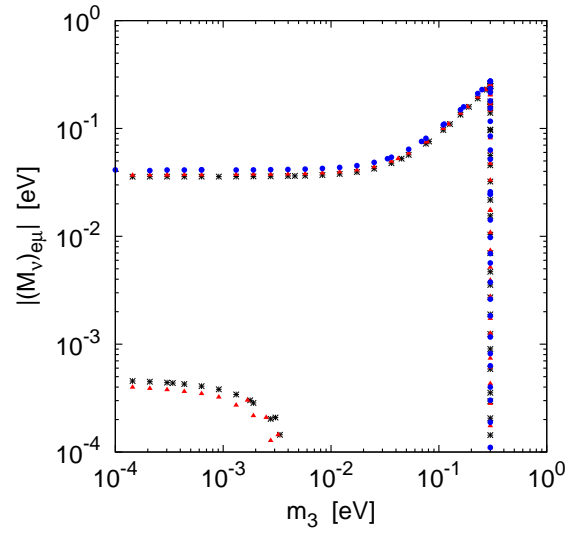
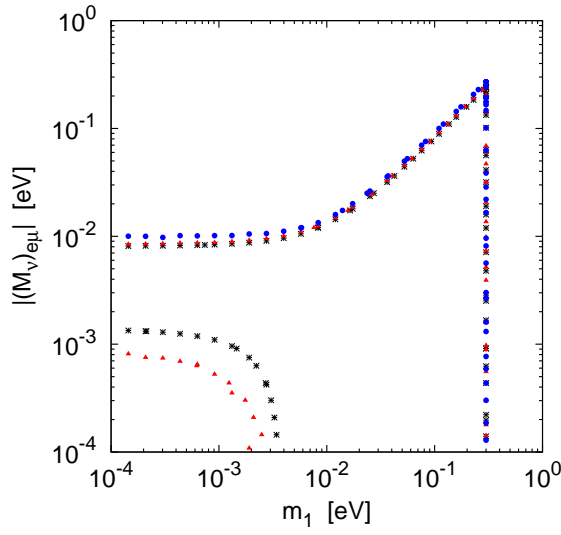
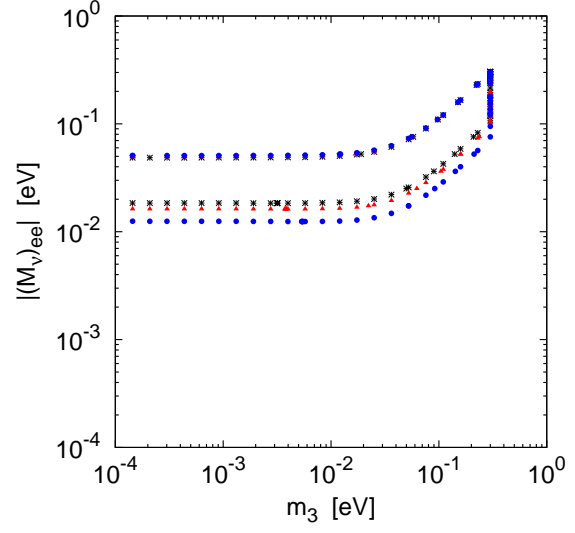
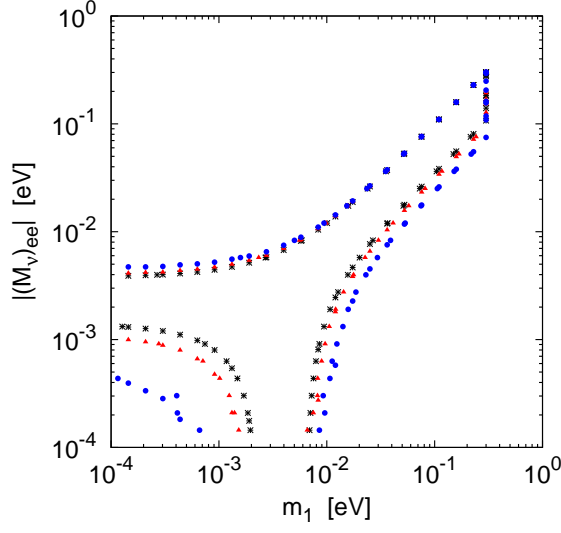
- [1] Y. Abe *et al.* (Double Chooz Coll.), *Indication for the disappearance of reactor electron antineutrinos in the Double Chooz experiment*, Phys. Rev. Lett. **108** (2012) 131801 [arXiv:1112.6353];
F.P. An *et al.* (Daya Bay Coll.), *Observation of electron-antineutrino disappearance at Daya Bay*, Phys. Rev. Lett. **108** (2012) 171803 [arXiv:1203.1669];
J.K. Ahn *et al.* (RENO Coll.), *Observation of reactor electron antineutrino disappearance in the RENO experiment*, Phys. Rev. Lett. **108** (2012) 191802 [arXiv:1204.0626].
- [2] K. Abe *et al.* (T2K Coll.), *Indication of electron neutrino appearance from an accelerator-produced off-axis muon neutrino beam*, Phys. Rev. Lett. **107** (2011) 041801 [arXiv:1106.2822];
P. Adamson *et al.* (MINOS Coll.), *Improved search for muon-neutrino to electron-neutrino oscillations in MINOS*, Phys. Rev. Lett. **107** (2011) 181802 [arXiv:1108.0015].
- [3] D.V. Forero, M. Tórtola and J.W.F. Valle, *Global status of neutrino oscillation parameters after recent reactor measurements*, arXiv:1205.4018v2; *Global status of neutrino oscillation parameters after Neutrino-2012*, Phys. Rev. D **86** (2012) 073012 [arXiv:1205.4018v3].
- [4] G.L. Fogli, E. Lisi, A. Marrone, D. Montanino, A. Palazzo and A.M. Rotunno, *Global analysis of neutrino masses, mixings and phases: entering the era of leptonic CP violation searches*, Phys. Rev. D **86** (2012) 013012 [arXiv:1205.5254v3].
- [5] A. Merle and W. Rodejohann, *The elements of the neutrino mass matrix: Allowed ranges and implications of texture zeros*, Phys. Rev. D **73** (2006) 073012 [hep-ph/0603111].
- [6] J. Beringer *et al.* (Particle Data Group), *Review of particle physics*, Phys. Rev. D **86** (2012) 010001.
- [7] G.C. Branco, L. Lavoura and J.P. Silva, *CP Violation*, Int. Ser. Monogr. Phys. **103** (1999) 1.

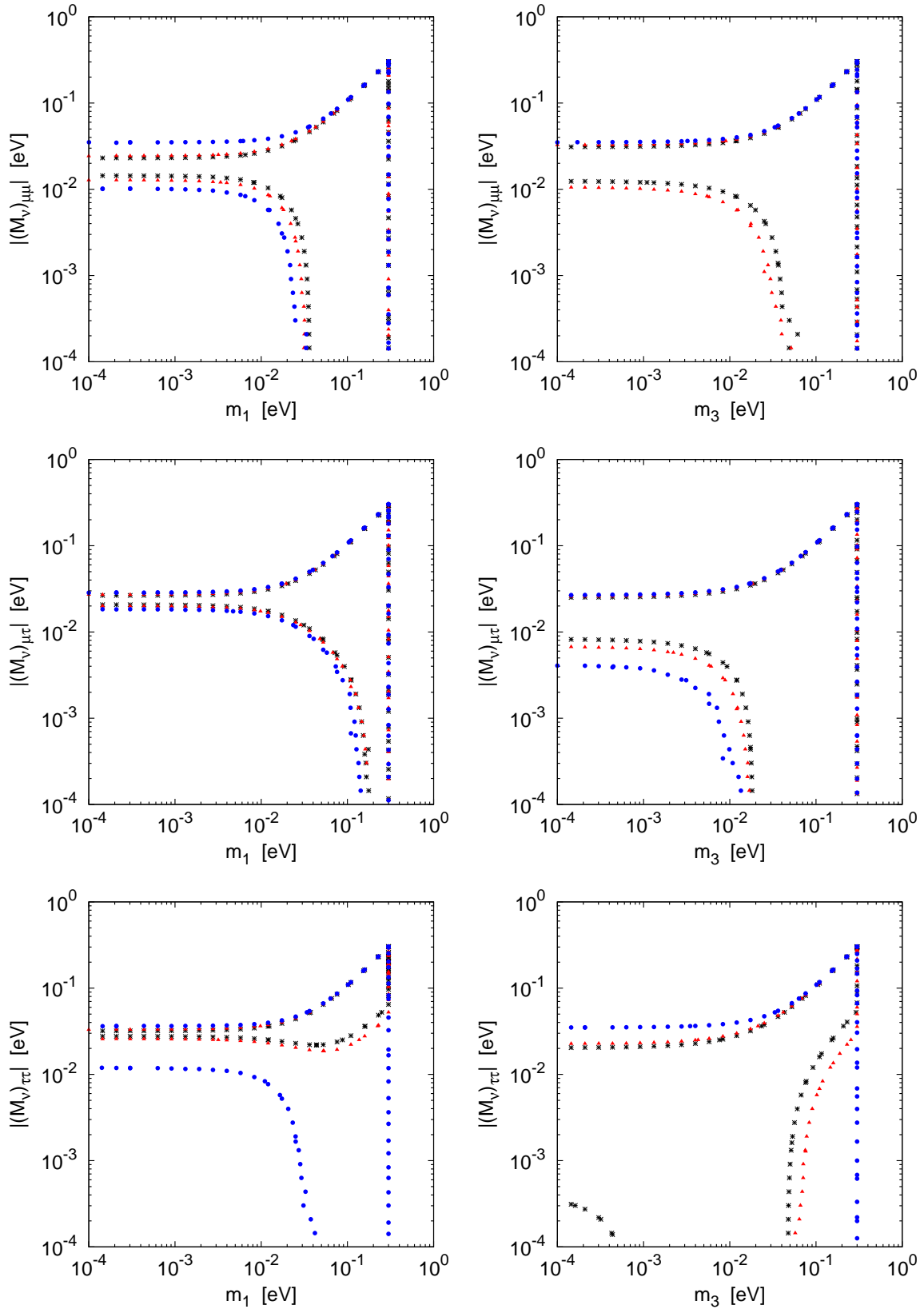
- [8] J.A. Nelder and R. Mead, *A simplex method for function minimization*, Comput. J. **7** (1965) 308.
- [9] W. Rodejohann, *Neutrinoless double beta decay and neutrino physics*, J. Phys. **G 39** (2012) 124008 [arXiv:1206.2560].
- [10] M. Auger *et al.* (EXO Coll.), *Search for Neutrinoless Double-Beta Decay in ^{136}Xe with EXO-200*, Phys. Rev. Lett. **109** (2012) 032505 [arXiv:1205.5608].
- [11] W. Grimus and P.O. Ludl, *Two-parameter neutrino mass matrices with two texture zeros*, arXiv:1208.4515.
- [12] P.H. Frampton, S.L. Glashow and D. Marfatia, *Zeroes of the neutrino mass matrix*, Phys. Lett. **B 536** (2002) 79 [hep-ph/0201008].

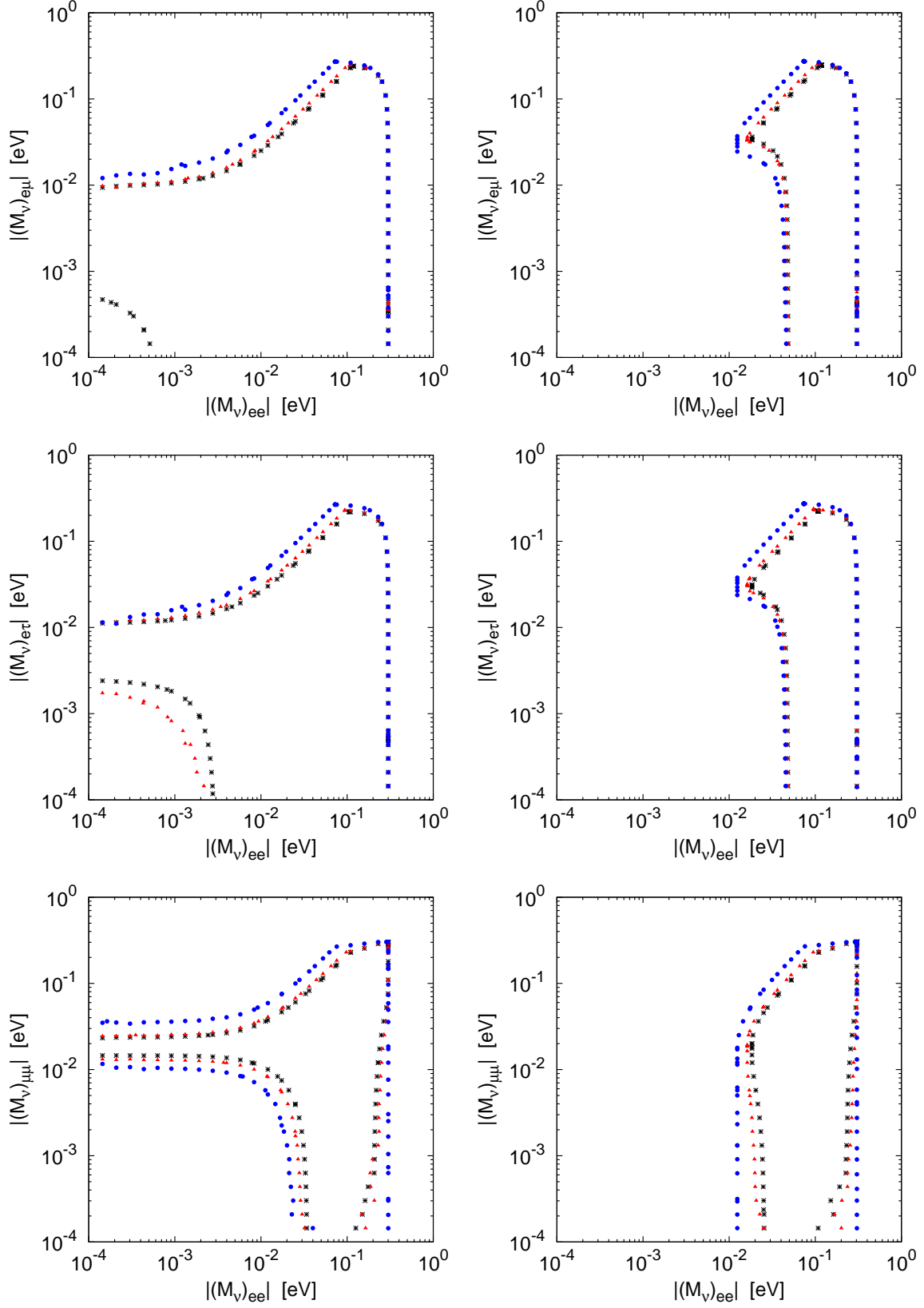
A Plots based on Fogli *et al.*

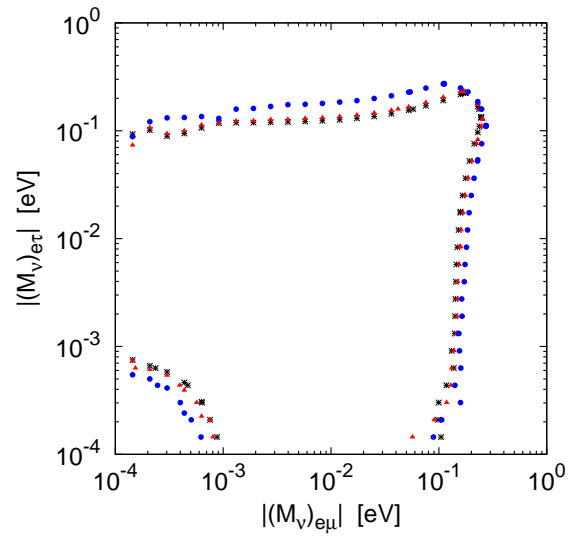
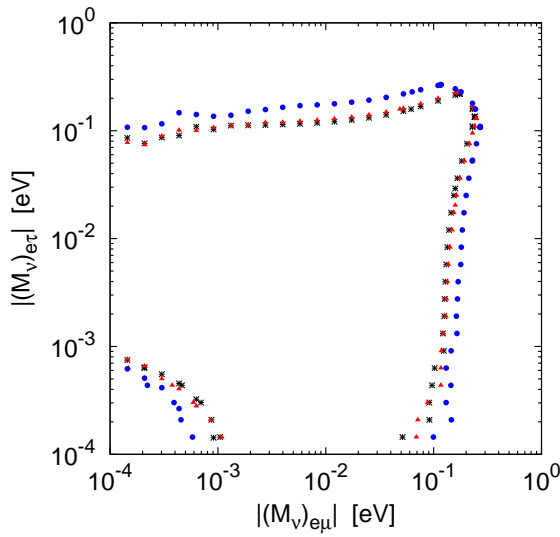
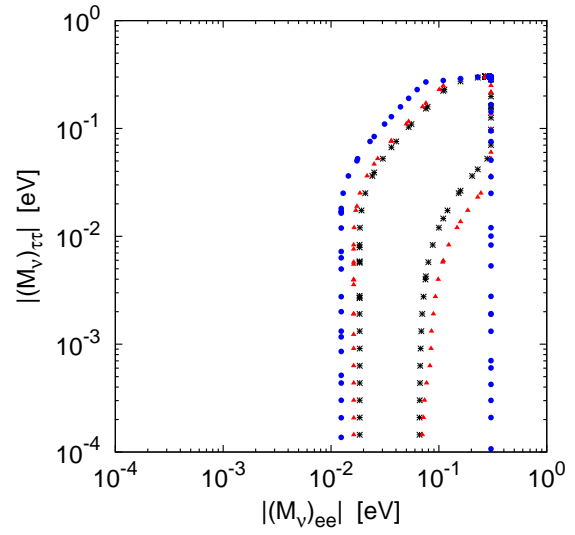
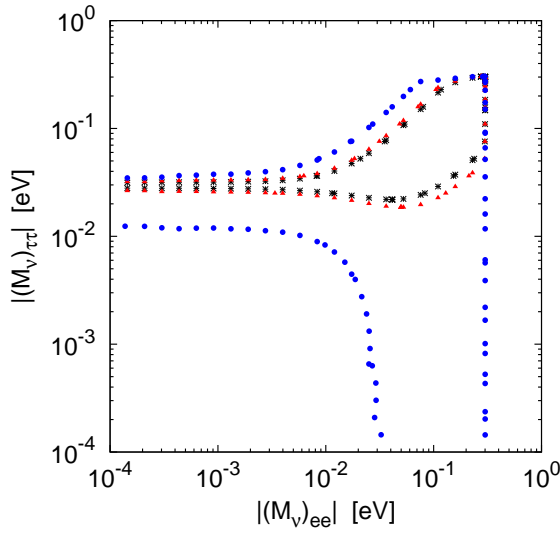
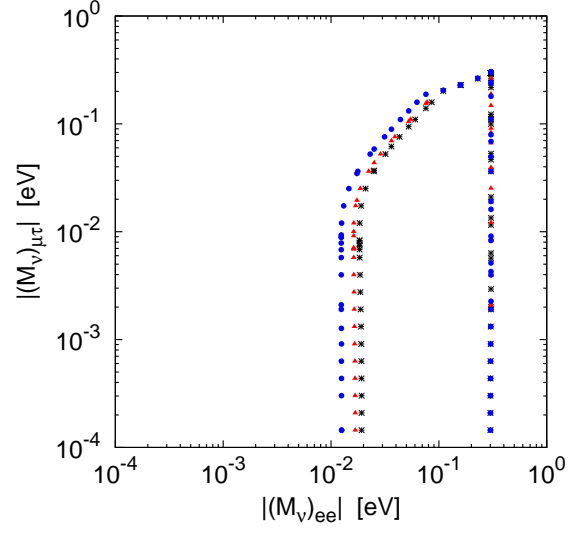
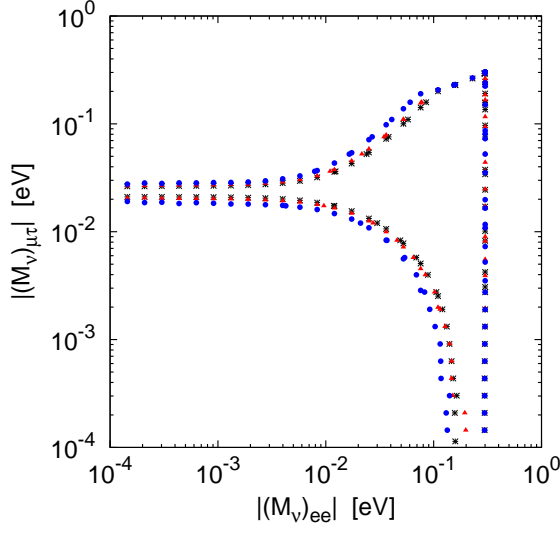
This appendix contains all 42 plots produced on the basis of the global fit by Fogli *et al.* [4].

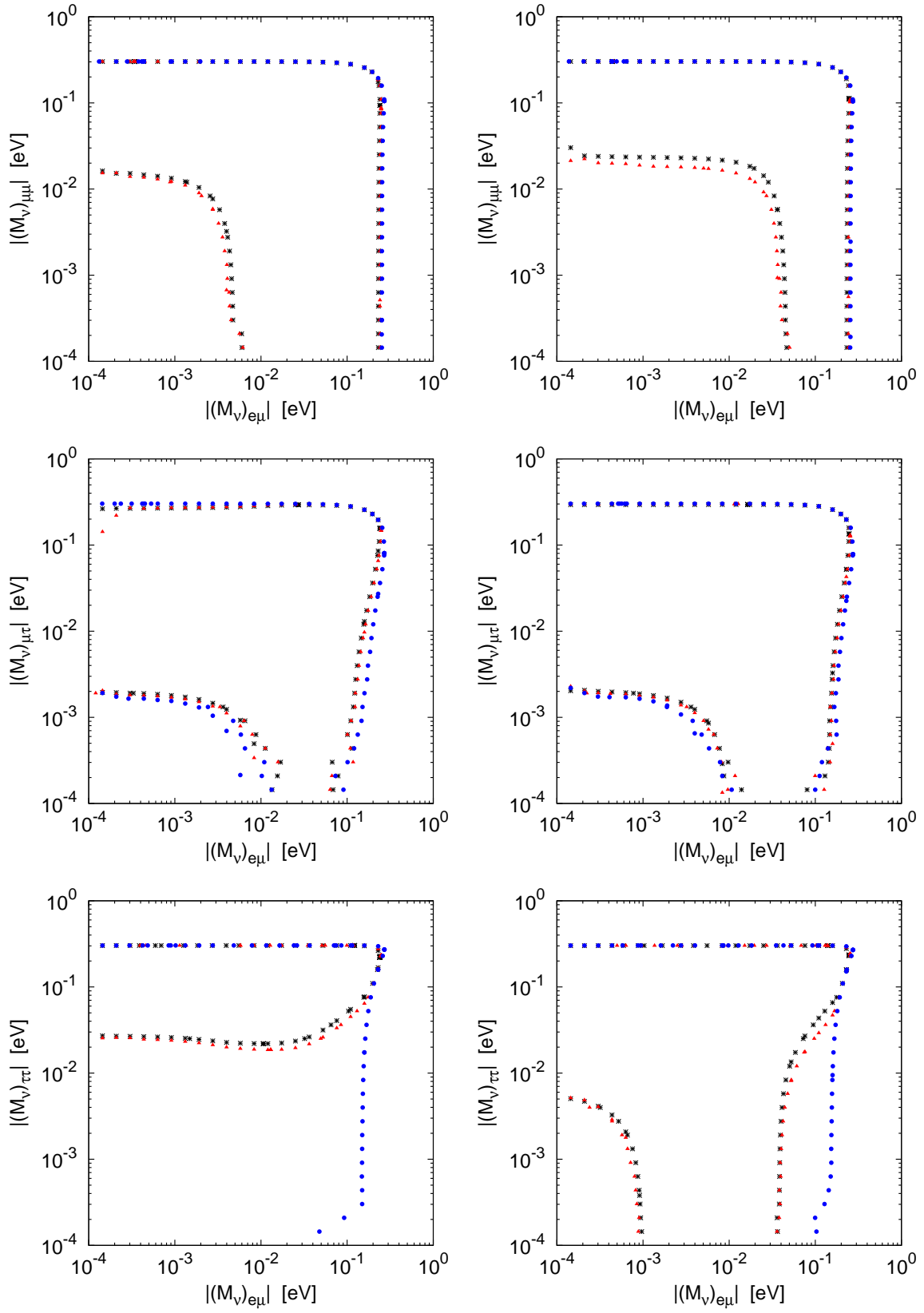
The figures in the left and right columns correspond to normal and inverted mass ordering, respectively. The plots consist of three types of points, each one describing the boundary of an allowed area. The best fit area is bounded by black stars *, the 1σ area is bounded by red triangles ▲, and finally the 3σ area is bounded by blue points ●. The same applies to the plots in appendices C and D.

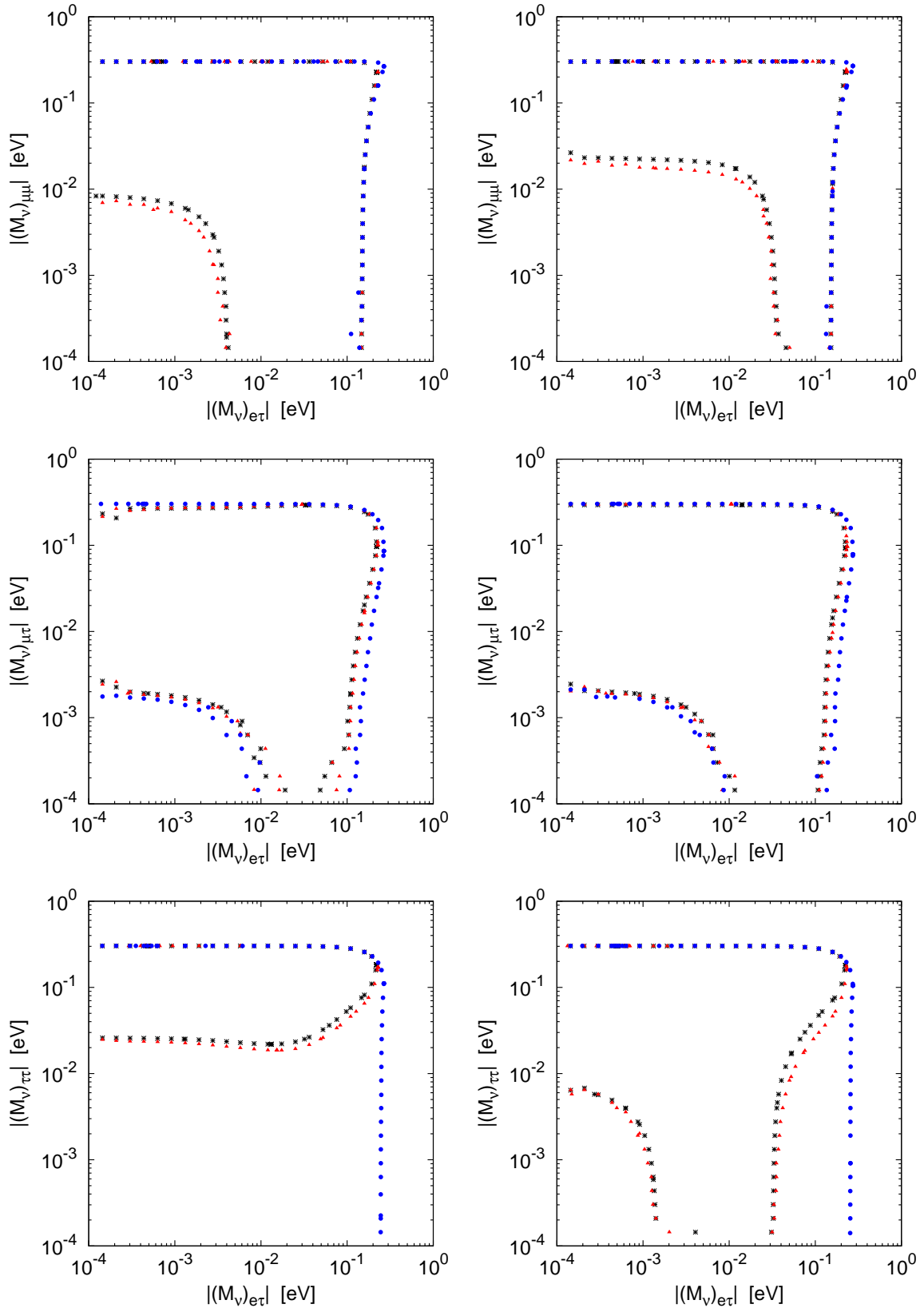


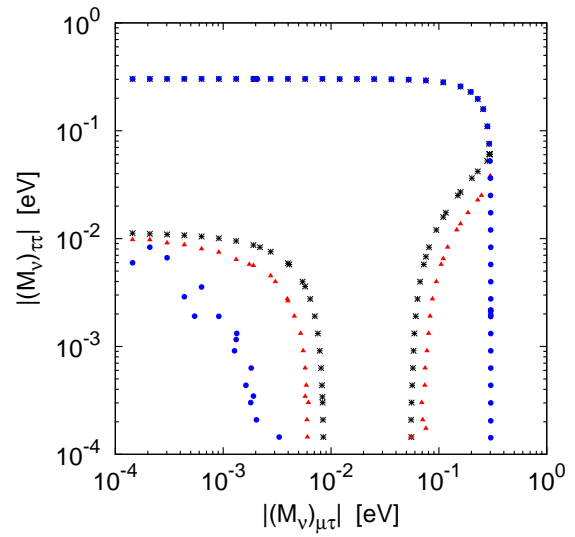
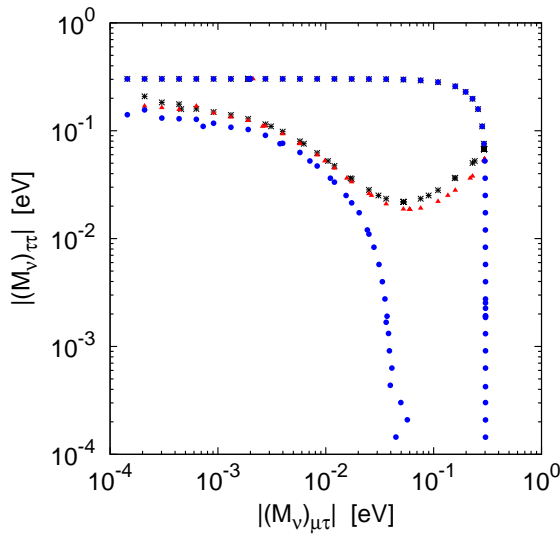
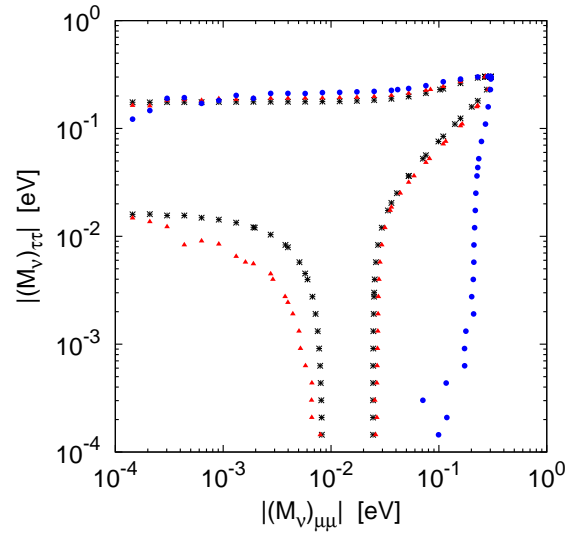
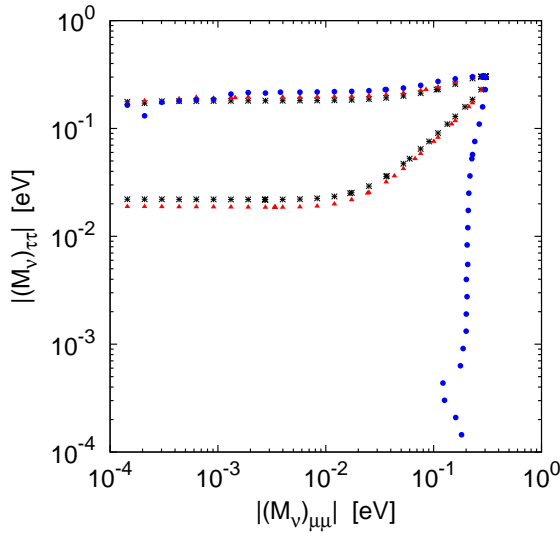
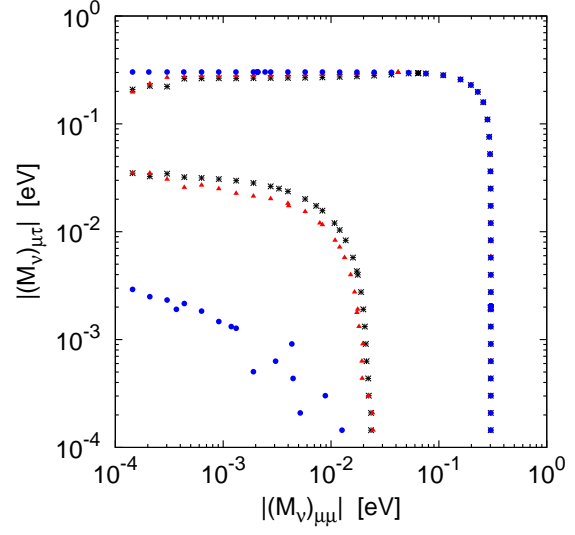
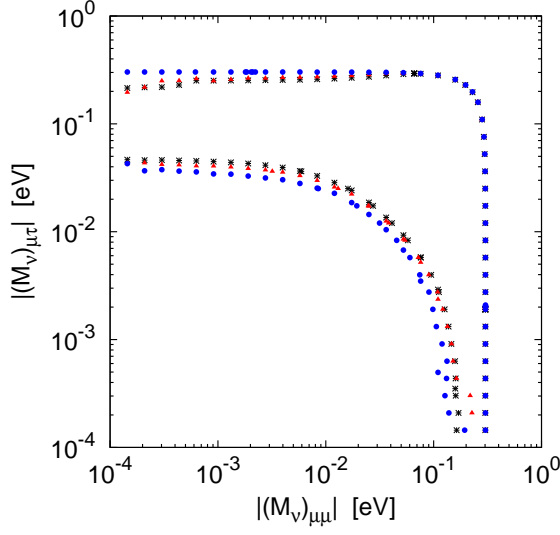








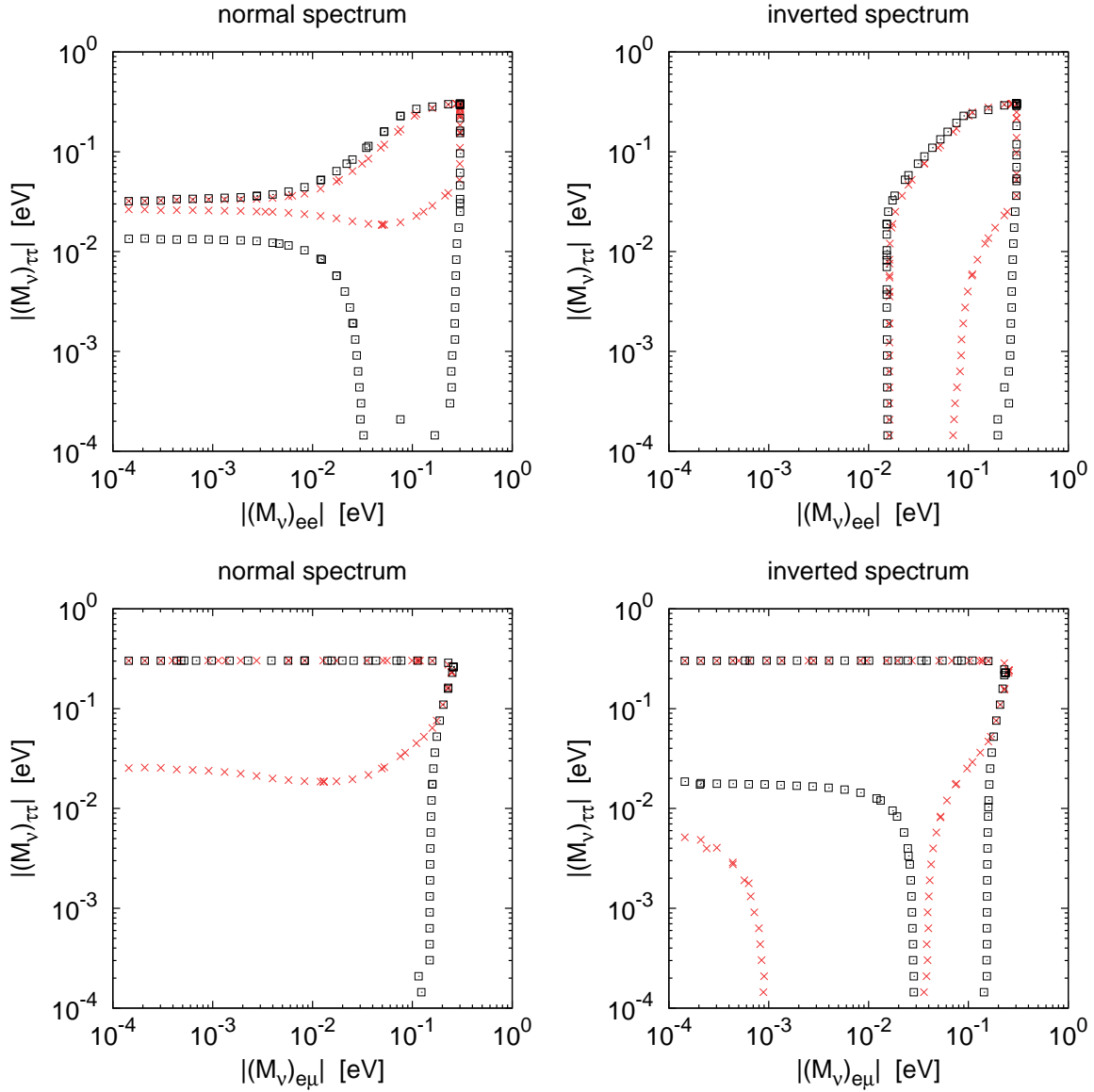


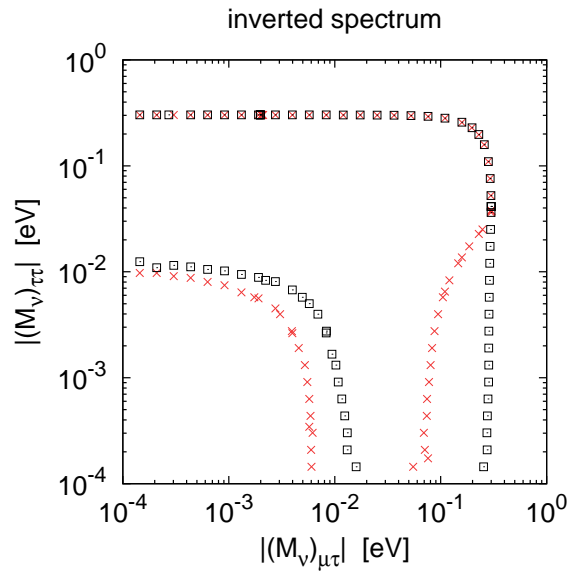
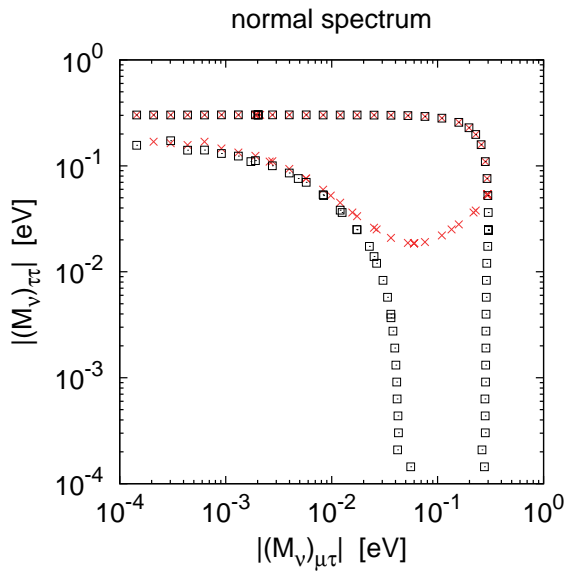
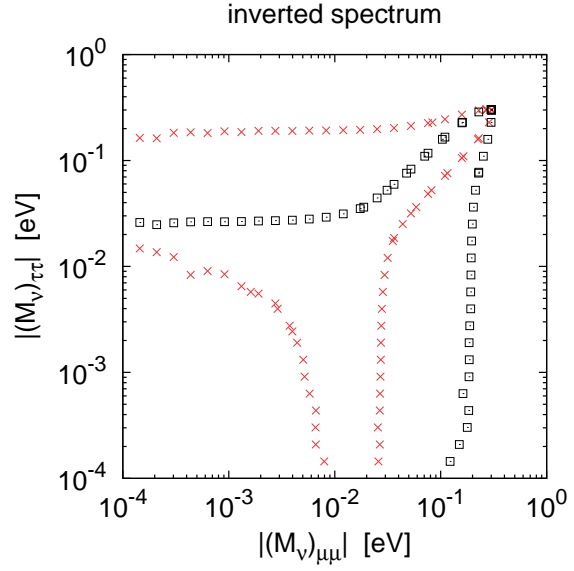
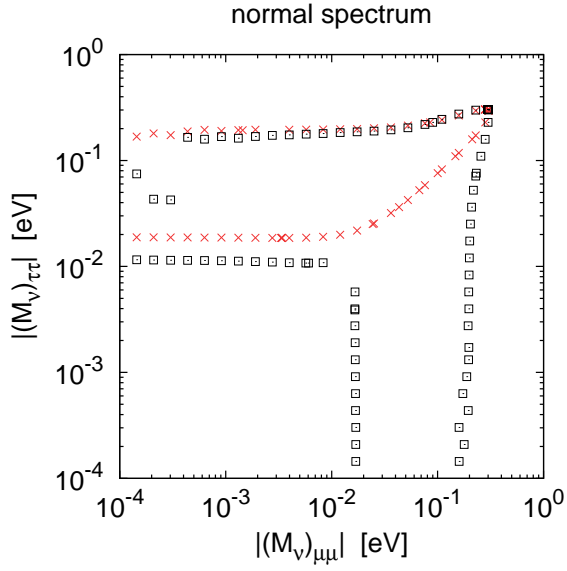
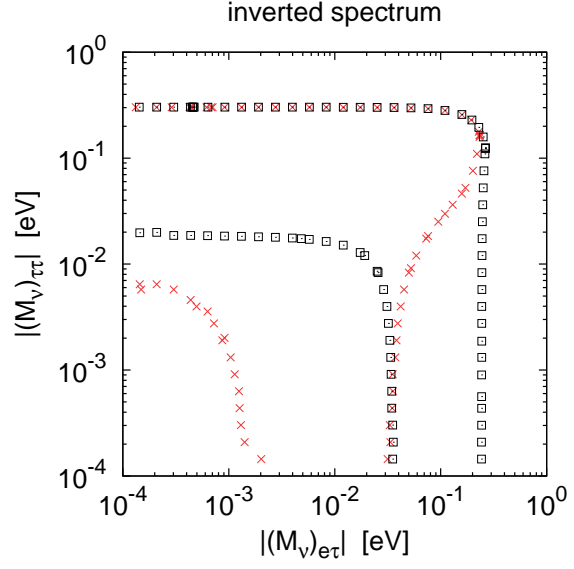
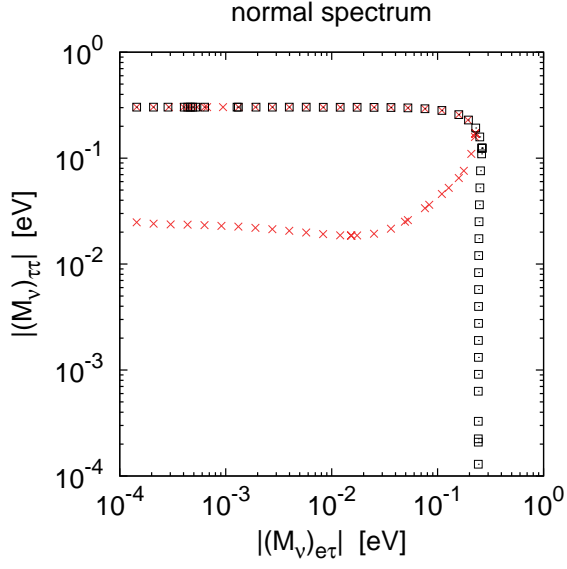


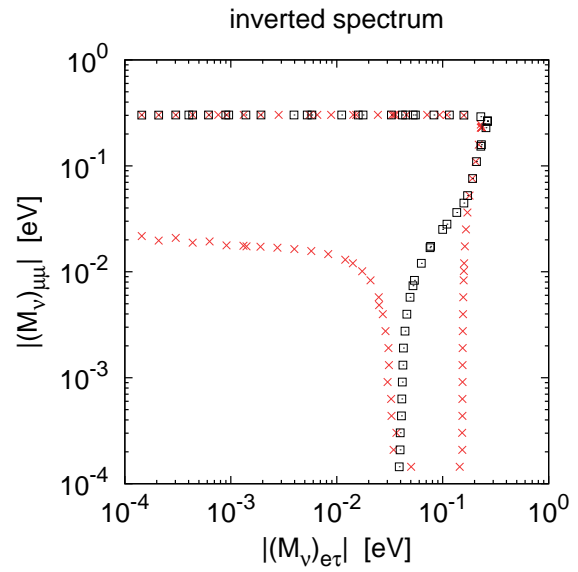
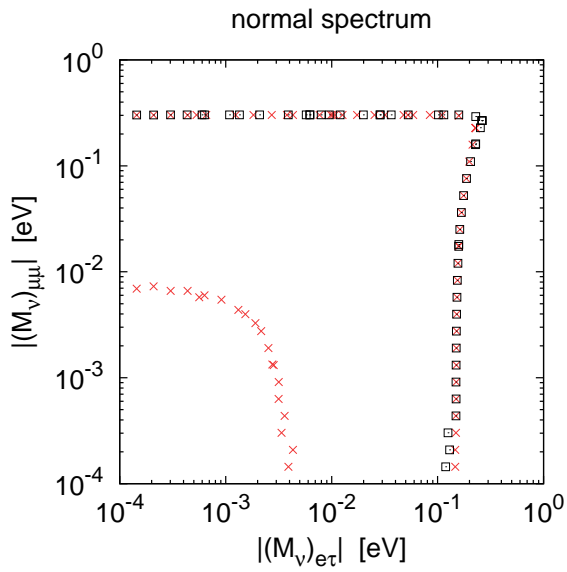
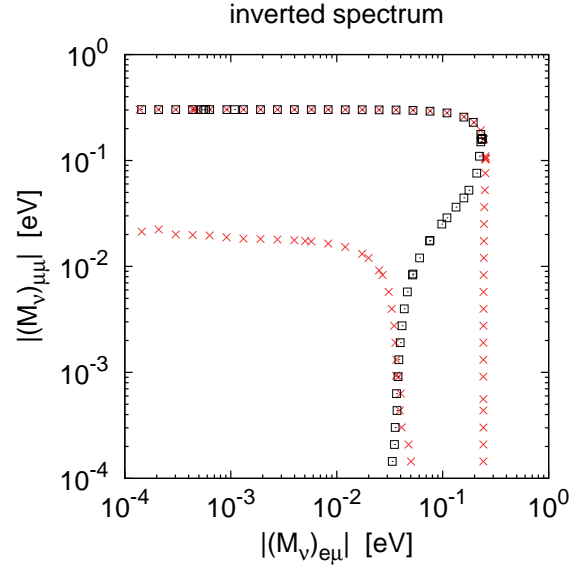
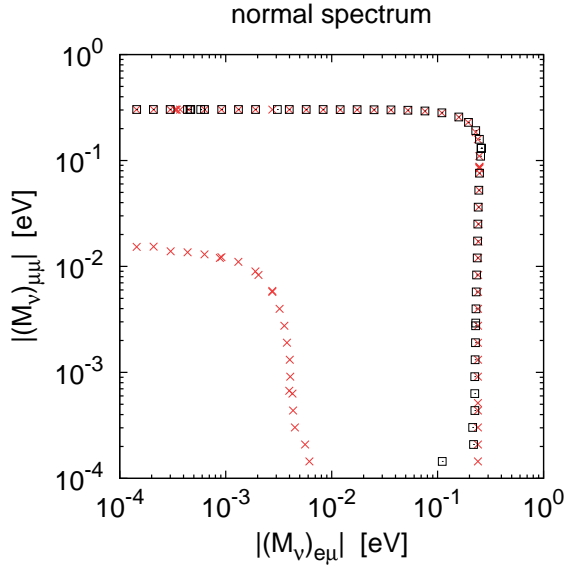
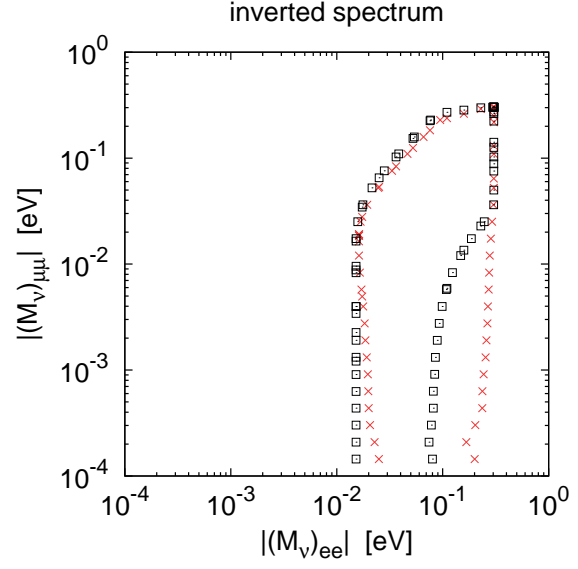
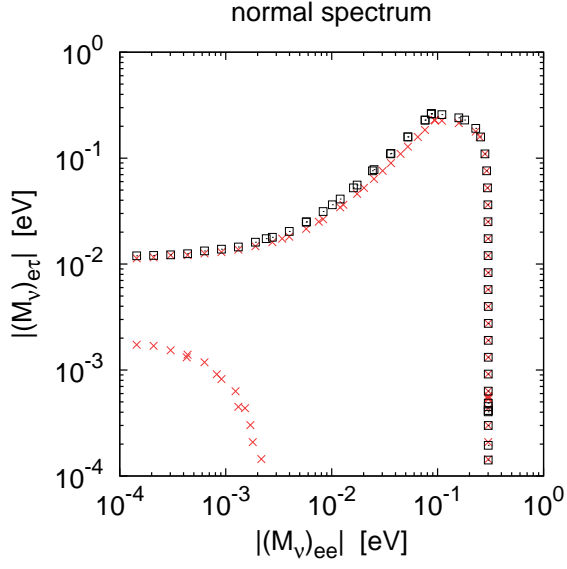
B Differences between the plots based on Fogli *et al.* and Forero *et al.* (version 3) at one sigma

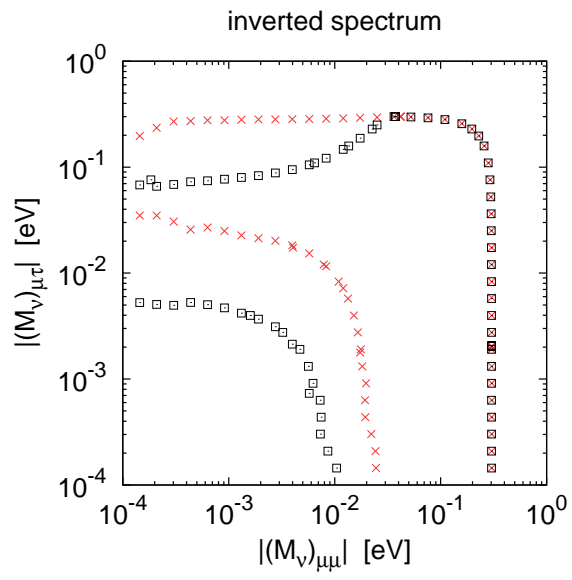
Here we present those correlations where there are notable differences between the plots based on Fogli *et al.* [4] and Forero *et al.* (version 3) [3] at the 1σ level. The following plots always contain the allowed 1σ areas for both Fogli *et al.* (bounded by red crosses \times) as well as Forero *et al.* (bounded by black boxes \square). The plot title shows the neutrino mass spectrum.

We begin with the ten correlation plots involving $|(\mathcal{M}_\nu)_{\tau\tau}|$. Afterwards we show the seven remaining plots.

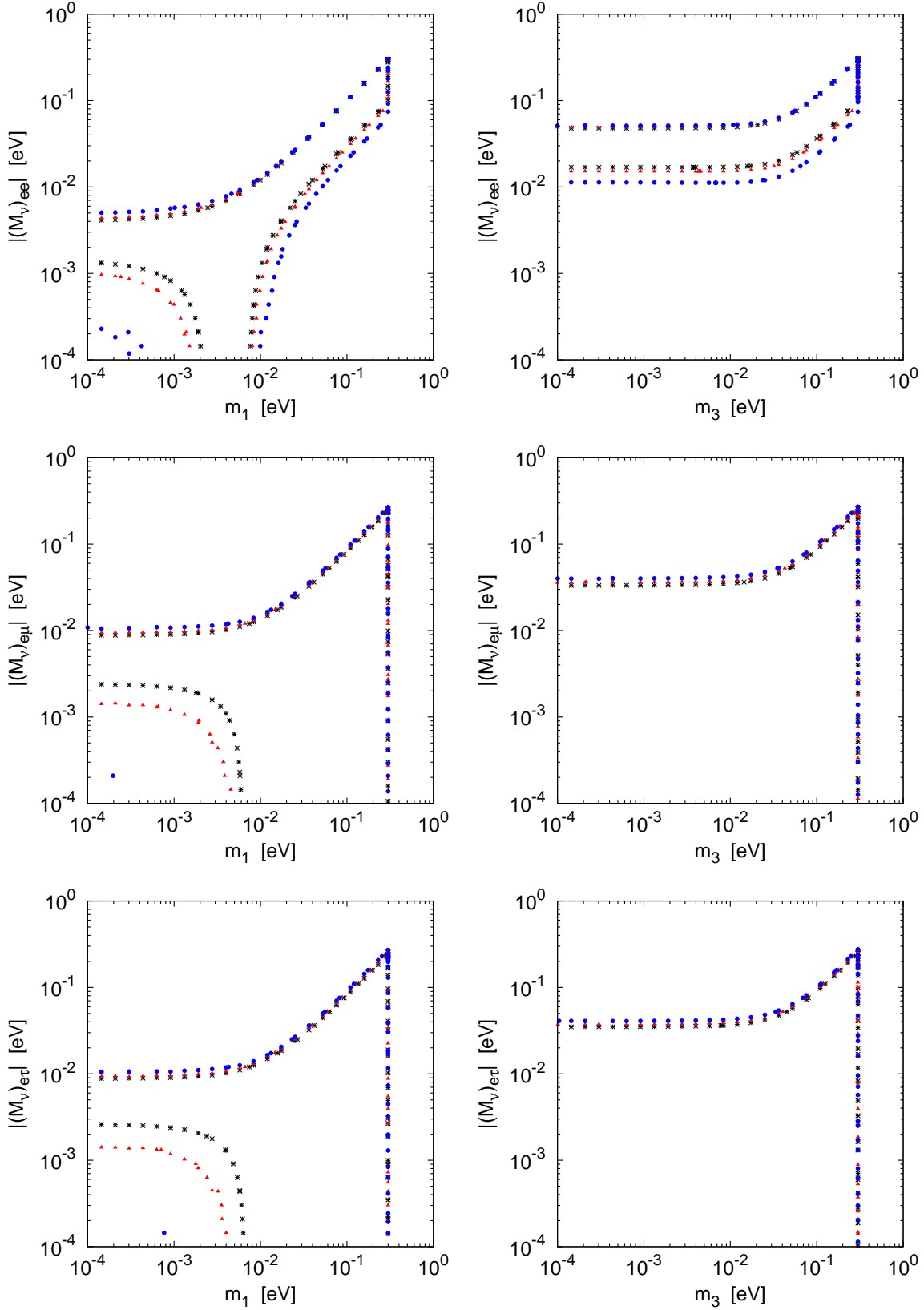


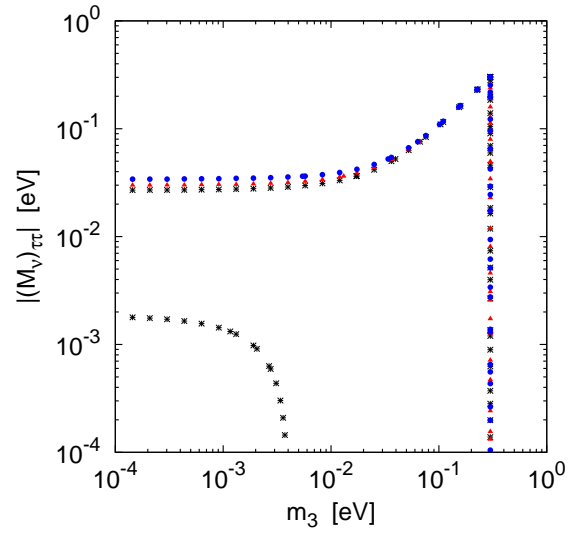
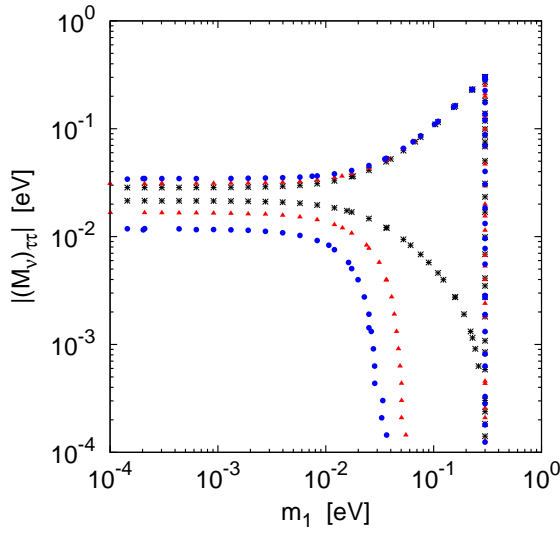
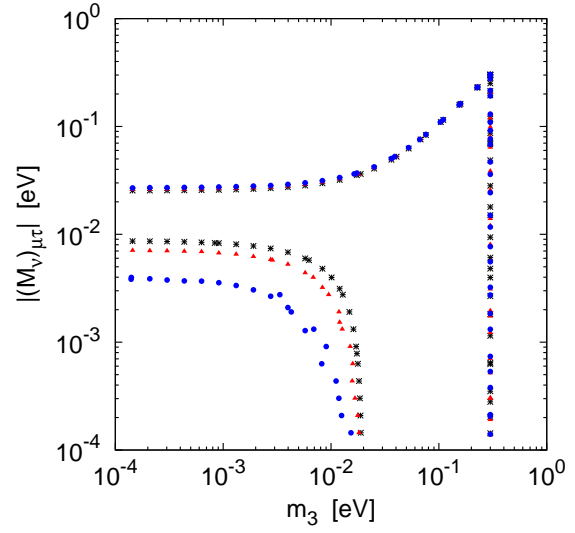
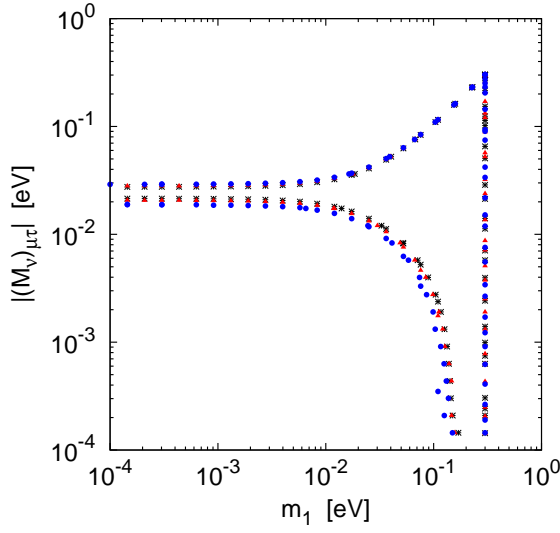
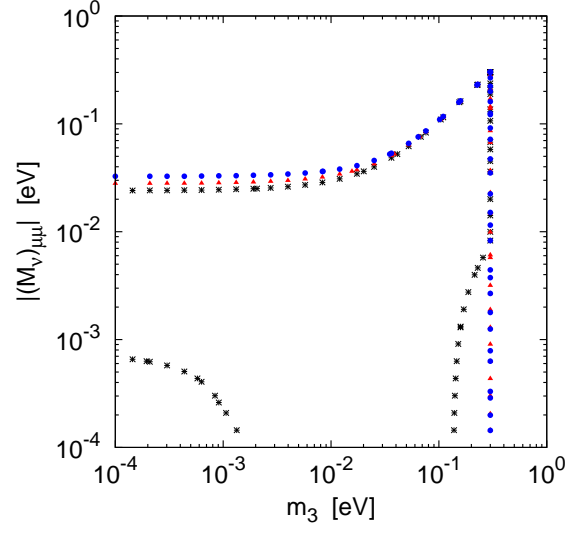
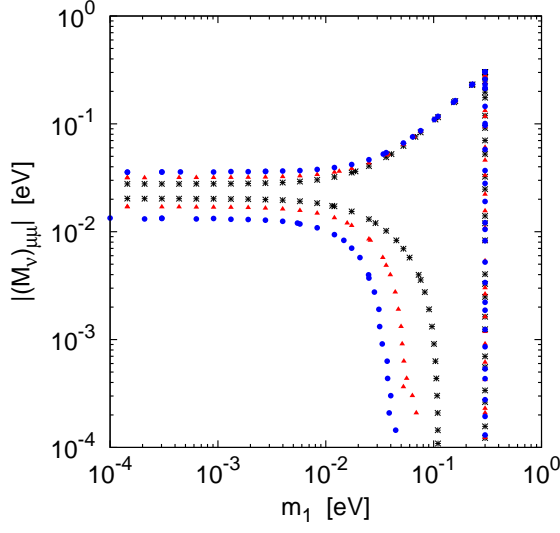


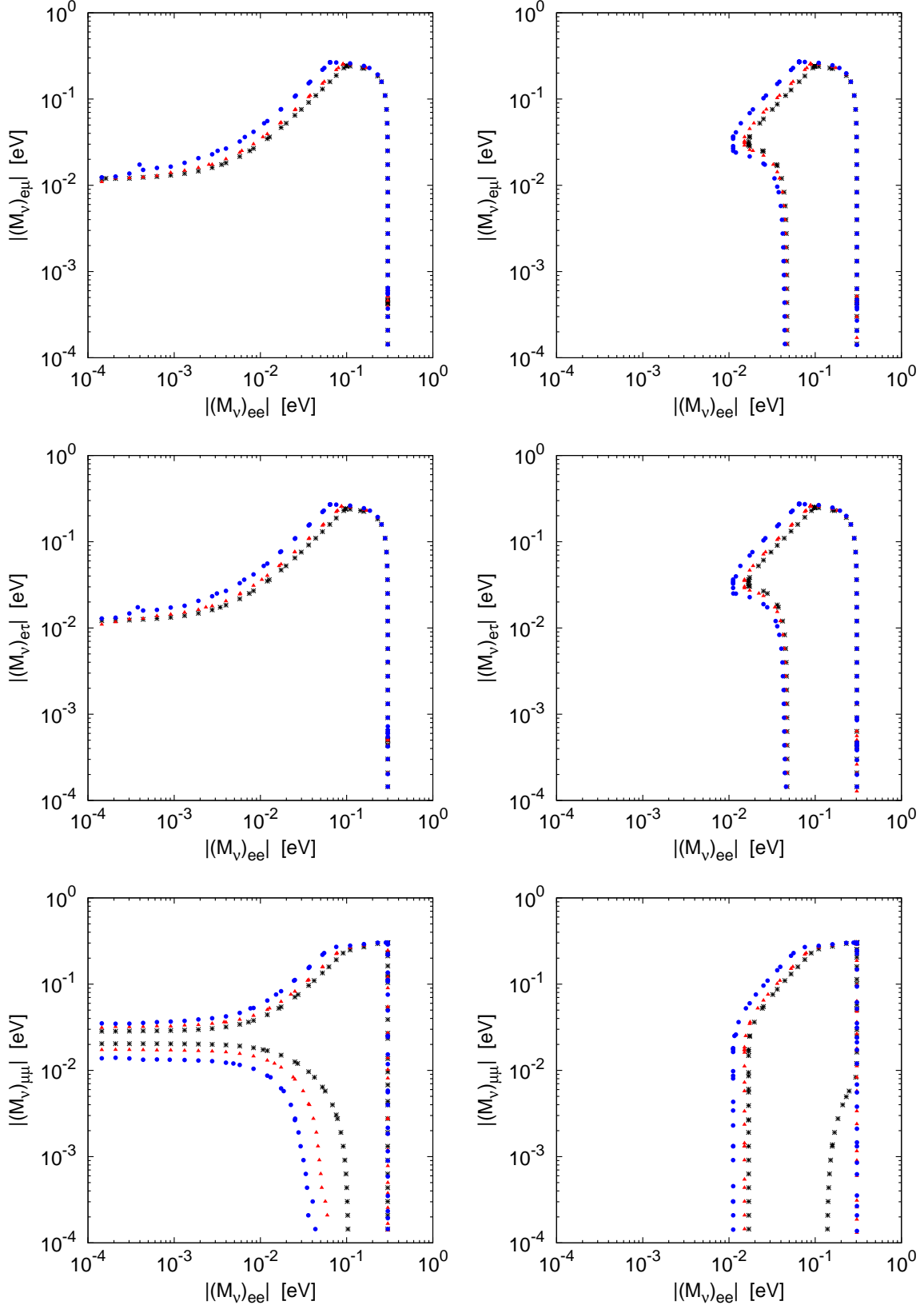


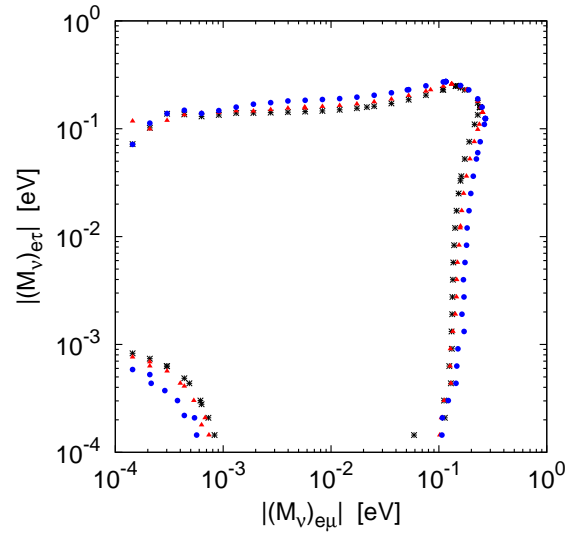
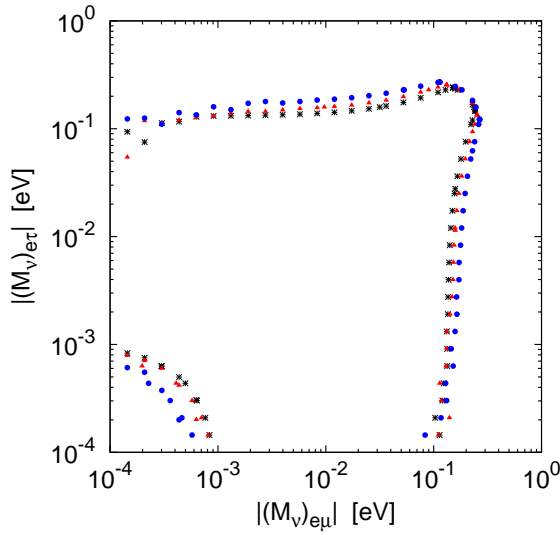
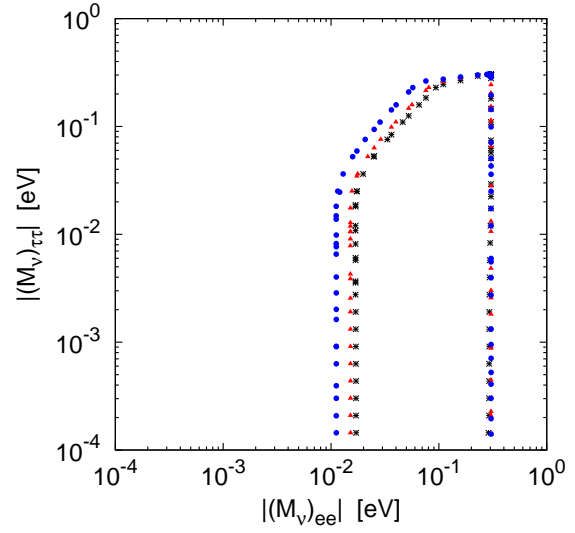
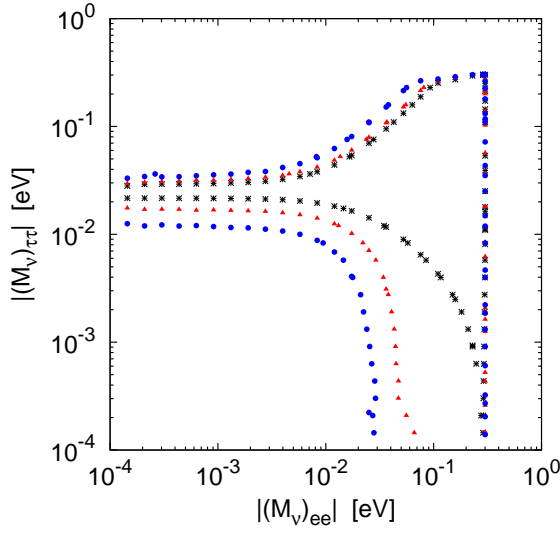
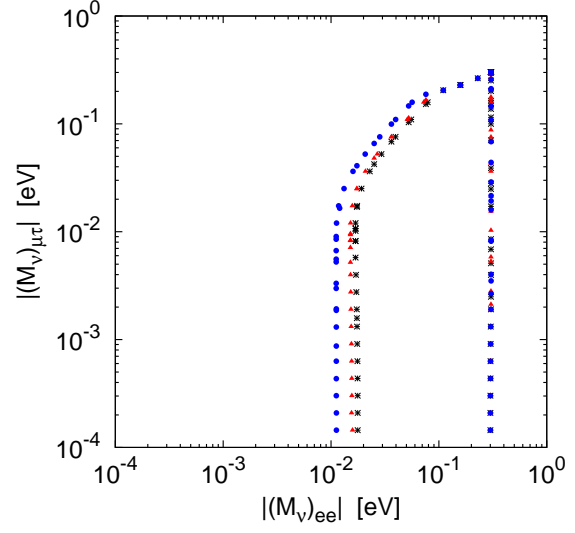
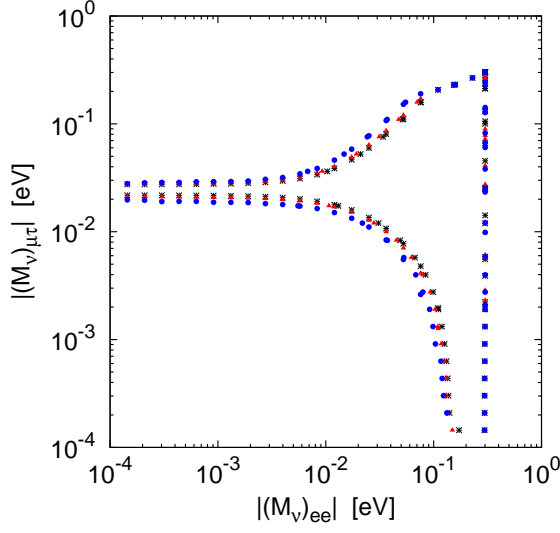


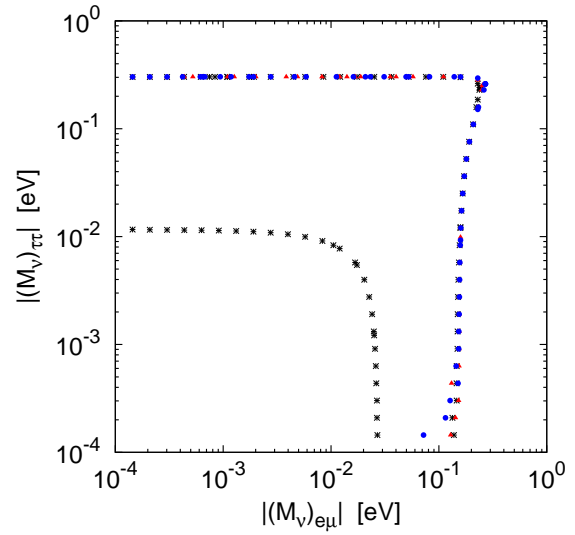
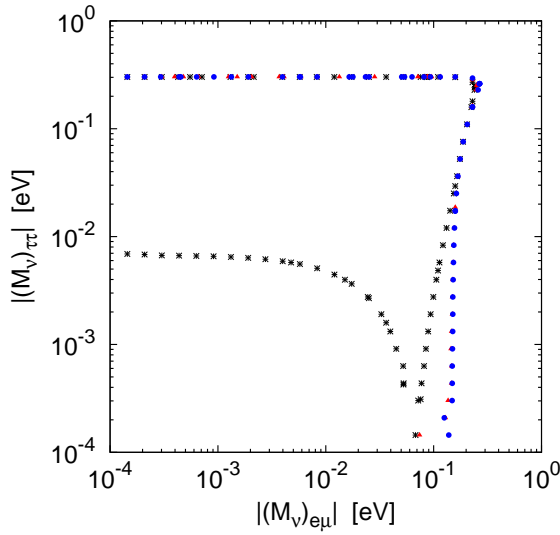
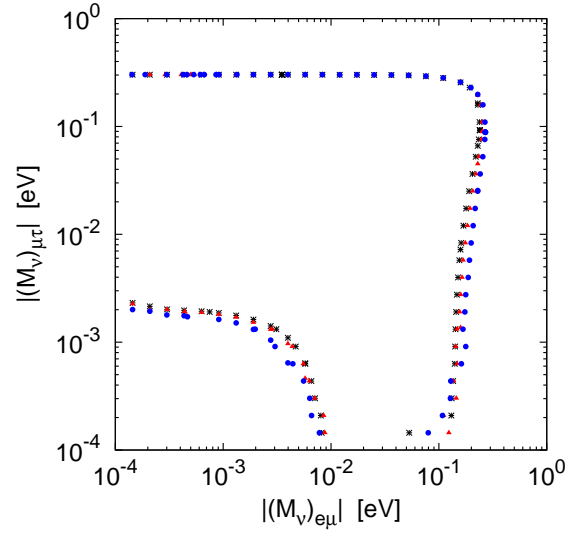
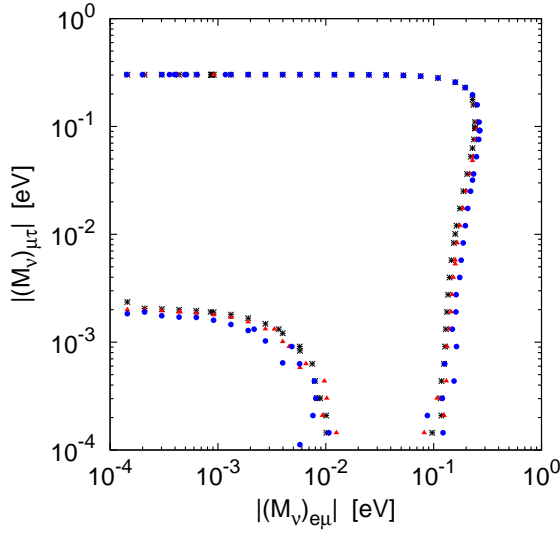
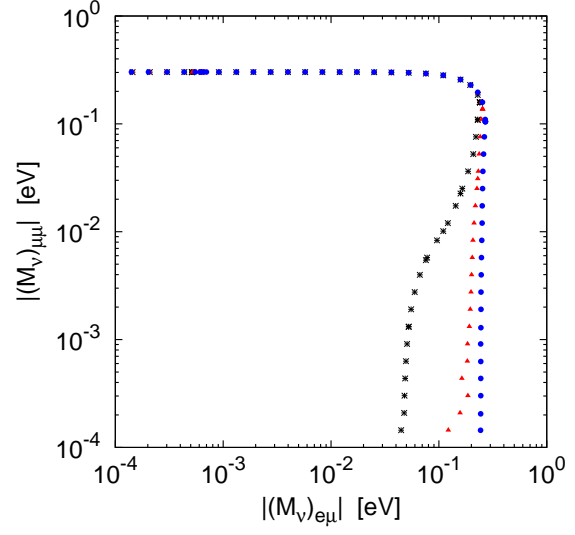
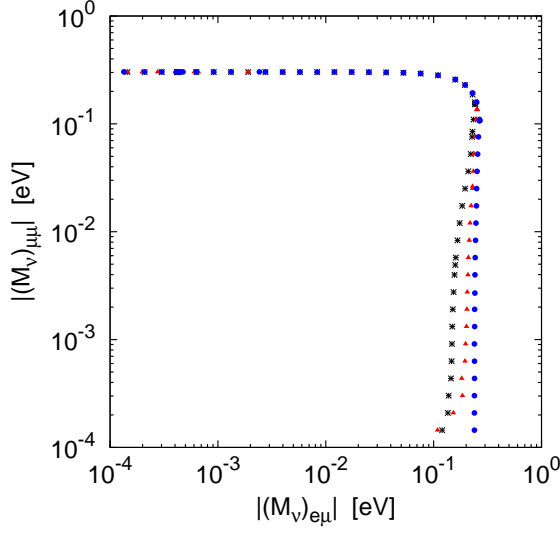
C Plots based on Forero *et al.* (version 2); *cf.* app. A

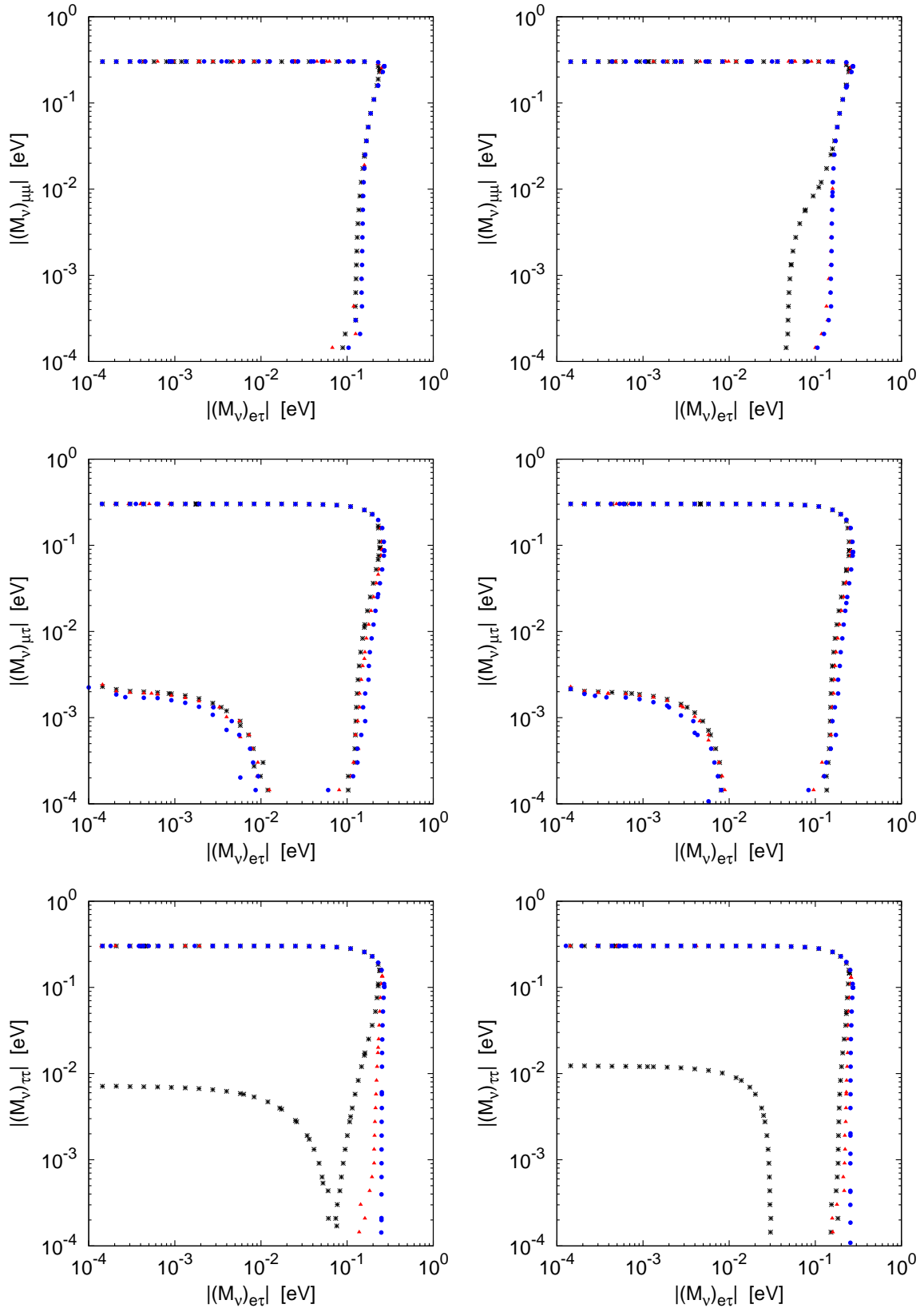


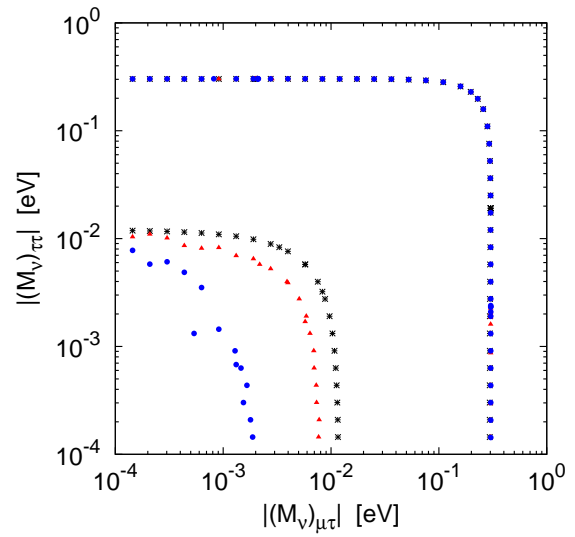
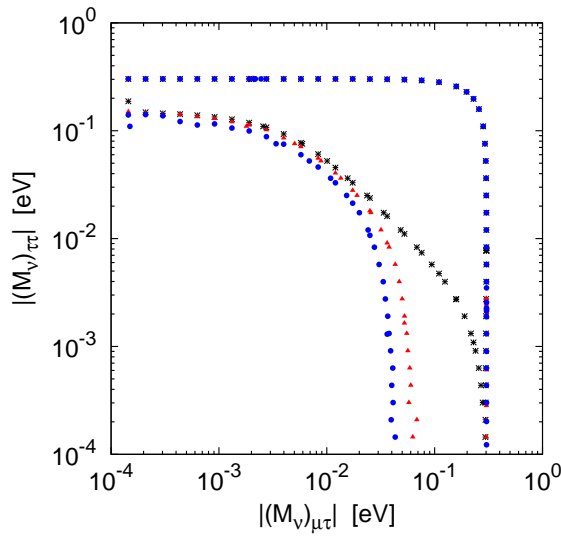
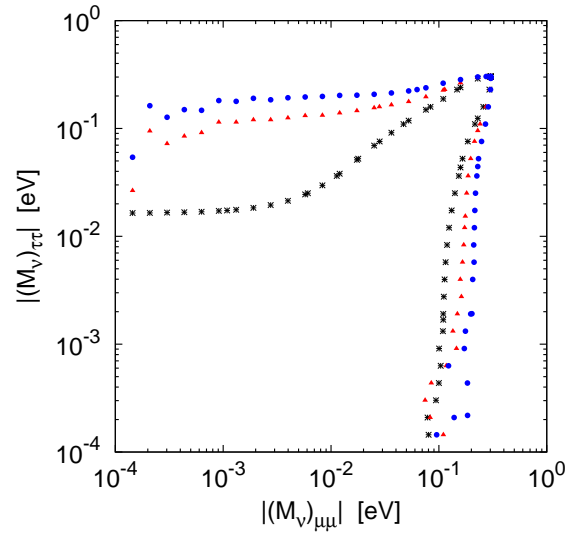
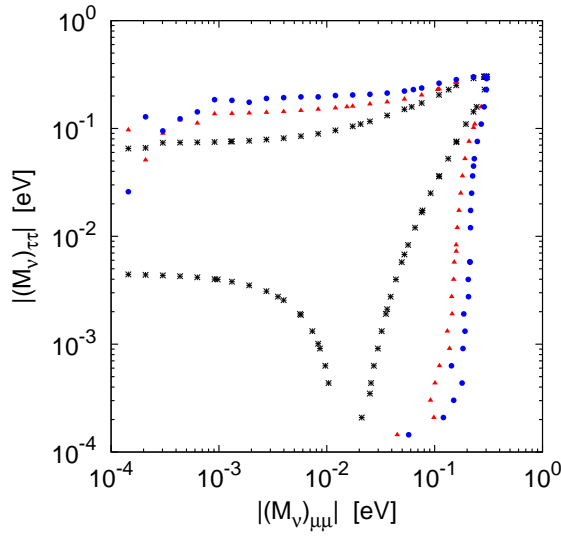
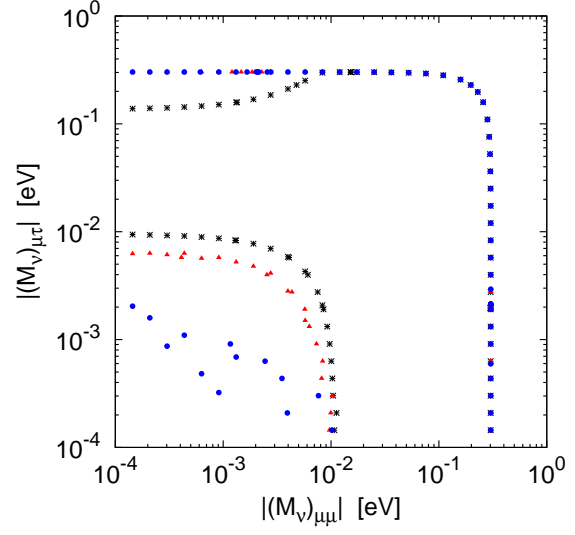
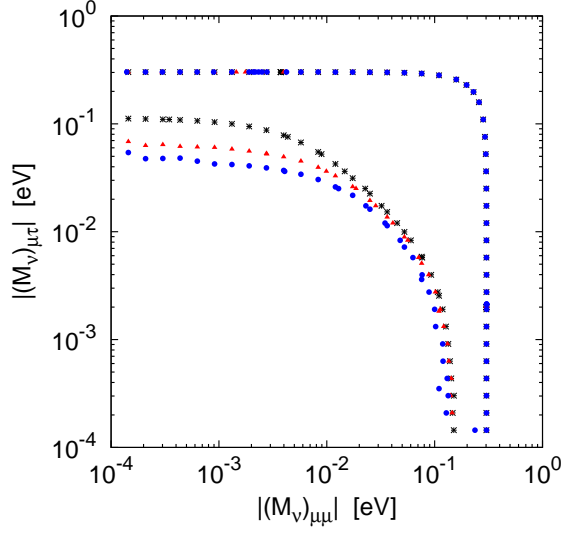












D Plots based on Forero *et al.* (version 3); *cf.* app. A

